

RESEARCH ARTICLE

Shigella sonnei infection of zebrafish reveals that O-antigen mediates neutrophil tolerance and dysentery incidence

Vincenzo Torraca^{1,2}, Myrsini Kaforou³, Jayne Watson⁴, Gina M. Duggan^{1,2}, Hazel Guerrero-Gutierrez¹, Sina Krokowski^{1,2}, Michael Hollinshead⁵, Thomas B. Clarke¹, Rafal J. Mostowy^{6,7}, Gillian S. Tomlinson⁸, Vanessa Sancho-Shimizu^{3,9}, Abigail Clements⁴, Serge Mostowy^{1,2*}

1 Section of Microbiology, MRC Centre for Molecular Bacteriology and Infection, Imperial College London, London, United Kingdom, **2** Department of Infection Biology, London School of Hygiene & Tropical Medicine, London, United Kingdom, **3** Department of Paediatrics, Division of Medicine, Imperial College London, London, United Kingdom, **4** Faculty of Natural Sciences, Department of Life Sciences, MRC Centre for Molecular Bacteriology and Infection, Imperial College London, London, United Kingdom, **5** Division of Virology, Department of Pathology, Cambridge University, Cambridge, United Kingdom, **6** Malopolska Centre of Biotechnology, Jagiellonian University, Krakow, Poland, **7** Faculty of Medicine, School of Public Health, Imperial College London, London, United Kingdom, **8** Division of Infection and Immunity, University College London, London, United Kingdom, **9** Department of Virology, Division of Medicine, Imperial College London, London, United Kingdom

* serge.mostowy@lshhtm.ac.uk



OPEN ACCESS

Citation: Torraca V, Kaforou M, Watson J, Duggan GM, Guerrero-Gutierrez H, Krokowski S, et al. (2019) *Shigella sonnei* infection of zebrafish reveals that O-antigen mediates neutrophil tolerance and dysentery incidence. PLoS Pathog 15(12): e1008006. <https://doi.org/10.1371/journal.ppat.1008006>

Editor: Matthew A. Mulvey, University of Utah, UNITED STATES

Received: July 24, 2019

Accepted: November 1, 2019

Published: December 12, 2019

Copyright: © 2019 Torraca et al. This is an open access article distributed under the terms of the [Creative Commons Attribution License](https://creativecommons.org/licenses/by/4.0/), which permits unrestricted use, distribution, and reproduction in any medium, provided the original author and source are credited.

Data Availability Statement: Raw sequencing data are deposited in GEO, the NCBI repository (accession: GSE140544).

Funding: V.T. is funded by the European Union's Horizon 2020 research and innovation program under the Marie Skłodowska-Curie (H2020-MSCA-IF-2015 – 700088). Work in the S.M. laboratory is supported by a European Research Council Consolidator Grant (772853 - ENTRAPMENT), Wellcome Trust Senior Research Fellowship

Abstract

Shigella flexneri is historically regarded as the primary agent of bacillary dysentery, yet the closely-related *Shigella sonnei* is replacing *S. flexneri*, especially in developing countries. The underlying reasons for this dramatic shift are mostly unknown. Using a zebrafish (*Danio rerio*) model of *Shigella* infection, we discover that *S. sonnei* is more virulent than *S. flexneri* *in vivo*. Whole animal dual-RNAseq and testing of bacterial mutants suggest that *S. sonnei* virulence depends on its O-antigen oligosaccharide (which is unique among *Shigella* species). We show *in vivo* using zebrafish and *ex vivo* using human neutrophils that *S. sonnei* O-antigen can mediate neutrophil tolerance. Consistent with this, we demonstrate that O-antigen enables *S. sonnei* to resist phagolysosome acidification and promotes neutrophil cell death. Chemical inhibition or promotion of phagolysosome maturation respectively decreases and increases neutrophil control of *S. sonnei* and zebrafish survival. Strikingly, larvae primed with a sublethal dose of *S. sonnei* are protected against a secondary lethal dose of *S. sonnei* in an O-antigen-dependent manner, indicating that exposure to O-antigen can train the innate immune system against *S. sonnei*. Collectively, these findings reveal O-antigen as an important therapeutic target against bacillary dysentery, and may explain the rapidly increasing *S. sonnei* burden in developing countries.

(206444/Z/17/Z), Wellcome Trust Research Career Development Fellowship (WT097411MA), and the Lister Institute of Preventive Medicine. The funders had no role in study design, data collection and analysis, decision to publish, or preparation of the manuscript.

Competing interests: The authors have declared that no competing interests exist.

Author summary

Shigella sonnei is predominantly responsible for dysentery in developed countries, and is replacing *Shigella flexneri* in areas undergoing economic development and improvements in water quality. Using *Shigella* infection of zebrafish (*in vivo*) and human neutrophils (*in vitro*), we discover that *S. sonnei* is more virulent than *S. flexneri* because of neutrophil tolerance mediated by its O-antigen oligosaccharide acquired from the environmental bacteria *Plesiomonas shigelloides*. To inspire new approaches for *S. sonnei* control, we show that increased phagolysosomal acidification or innate immune training can promote *S. sonnei* clearance by neutrophils *in vivo*. These findings have major implications for our evolutionary understanding of *Shigella*, and may explain why exposure to *P. shigelloides* in low and middle-income countries (LMICs) can protect against dysentery incidence.

Introduction

Shigella is the causative agent of bacillary dysentery (also called shigellosis), resulting from invasion of the intestinal epithelium and leading to ~164000 deaths annually [1,2]. The Global Enteric Multicenter Study (GEMS) is the largest study ever conducted on diarrhoeal diseases in developing countries (i.e. areas undergoing economic development and improvements in water quality), enrolling > 20000 children from seven countries across Asia and Africa, and identified *Shigella* as a major cause of diarrhoea in children < 5 years old [3]. *Shigella* is also recognised by the World Health Organization as a priority pathogen exhibiting antimicrobial resistance [4,5]. The emergence of multidrug resistant bacteria and the lack of effective vaccines has resulted in a desperate need to understand *Shigella* pathogenesis and identify new approaches for infection control. In the lab, infection with *Shigella flexneri* has been a valuable discovery tool in the field of innate immunity, helping to illuminate the role of neutrophil extracellular traps (NETs) [6], nucleotide-binding oligomerisation domain (NOD)-like receptors (NLRs) [7], bacterial autophagy [8], interferon-inducible guanylate-binding proteins (GBPs) [9,10] and septin-mediated cell-autonomous immunity [11,12] in host defence.

The genus *Shigella* comprises four different species (*S. flexneri*, *S. sonnei*, *S. boydii*, *S. dysenteriae*), although DNA sequencing suggests they evolved from convergent evolution of different founders [13]. The most recent strains of *S. flexneri* emerged from *Escherichia coli* >35000 years ago [13], while *S. sonnei* (a monoclonal strain) emerged from *E. coli* in central Europe ~500 years ago [14]. *S. flexneri* is historically regarded as the primary agent of dysentery worldwide, yet *S. sonnei* has recently become the most prevalent cause of dysentery in developing countries [15,16]. Reasons for this dramatic shift are mostly unknown. Hypotheses include improved water sanitation leading to reduced cross-immunisation by *Plesiomonas shigelloides* (which carries an O-antigen oligosaccharide identical to *S. sonnei*) [16,17], as well as a type VI secretion system (T6SS)-mediated competitive advantage that *S. sonnei* exerts over *S. flexneri* and the Gram-negative gut microbiome for niche occupancy [18].

Except for non-human primates, there is no mammalian model that fully recapitulates human shigellosis. The zebrafish model is increasingly being used to study human bacterial pathogens *in vivo*, including *S. flexneri* [19,20]. The major pathogenic events that lead to shigellosis in humans (i.e., macrophage cell death, invasion and multiplication within epithelial cells, cell-to-cell spread, inflammatory destruction of the host epithelium) are recapitulated in a zebrafish model of *S. flexneri* infection [21]. Exploiting the optical accessibility of zebrafish larvae, it is possible to spatio-temporally examine the development, coordination and resolution of the innate immune response to *S. flexneri in vivo*. As a result, *S. flexneri*-zebrafish

infection has been useful to illuminate key roles for bacterial autophagy [22], bacterial predation [23], inflammation [24] and trained innate immunity [25] in host defence *in vivo*.

How *S. sonnei* infection differs from *S. flexneri* infection is poorly understood, yet clinical management of both infections is the same. Here, we develop a *S. sonnei*-zebrafish infection model and discover that *S. sonnei* is more virulent than *S. flexneri in vivo* because of neutrophil tolerance mediated by its O-antigen. We show that increased phagolysosomal acidification or innate immune training can promote *S. sonnei* clearance by neutrophils *in vivo*. These results may inspire new approaches for *S. sonnei* control.

Results

S. sonnei is more virulent than *S. flexneri* in a zebrafish infection model

To compare the virulence of *S. flexneri* and *S. sonnei in vivo*, we injected *S. flexneri* M90T or *S. sonnei* 53G in the hindbrain ventricle (HBV) of zebrafish larvae at 3 days post-fertilisation (dpf). Unexpectedly, *S. sonnei* led to significantly more zebrafish death and higher bacterial burden, as compared to *S. flexneri* (Fig 1A and 1B). The majority of larvae inoculated with <600 CFU of *S. sonnei* survive, whereas the majority of larvae inoculated with >1500 CFU of *S. sonnei* die by 72 hpi (S1A and S1B Fig). In agreement with being more virulent, *S. sonnei* infected larvae have significantly increased expression of key inflammatory markers at 6 and 24 hpi, as compared to *S. flexneri* infected larvae (Fig 1C and 1D). Moreover, *S. sonnei*, unlike *S. flexneri*, disseminates out of the HBV into the neuronal tube and bloodstream (Fig 1E and 1F, S1C–S1F Fig). The increased virulence of *S. sonnei* is also observed using an intravenous route of infection (S1G and S1H Fig), using human clinical isolates of bacteria (S1I and S1J Fig) and when infected larvae are incubated at 28.5°C, 32.5°C or 37°C (Fig 1A and 1B, S1K–S1N Fig). Therefore, we used *S. sonnei* 53G infection of the HBV incubated at 28.5°C (the standard temperature for zebrafish maintenance) for the rest of our study (unless specified otherwise). Taken together, using multiple infection routes, bacterial strains and temperatures, these data show for the first time that *S. sonnei* is significantly more virulent than *S. flexneri in vivo*.

Whole animal dual-RNAseq profiling of *S. sonnei* infected larvae

The transcriptional signature of *Shigella in vivo* was mostly unknown. We performed whole animal dual-RNAseq profiling of *S. sonnei* infected larvae by isolating whole RNA at 24 hpi and mapping reads to both *Shigella* and zebrafish genomes (Fig 2A). RNA isolated from Log phase (OD₆₀₀ ~0.6) bacterial culture grown at 28.5°C was used as baseline for the identification of differential expression in the bacterial transcriptome. RNA isolated from PBS-injected larvae was used as baseline for the identification of differential expression in the host transcriptome. Gene count data was obtained for both the host and pathogen, and statistical analysis was performed using DESeq2 (see dedicated section in Materials and Methods). Genes were considered significantly differentially expressed if Log₂(Fold Change) > 1 or < -1 and the adjusted p value < 0.05. Principal component analysis (PCA) was employed for *S. sonnei* and larval count data separately, and these plots confirm the clustering between biological replicates according to their state (S2A and S2B Fig). After performing differential expression analysis between infected and control states, we found 1538 differentially expressed *S. sonnei* genes (representing ~1/3 of the *S. sonnei* 53G genome, Fig 2B, see also S1 Table and S2 Fig for in-depth exploration) and 337 differentially expressed zebrafish genes (Fig 2C, see also S2 Table and S2 Fig for in-depth exploration). In the case of *S. sonnei*, 878 genes are significantly up-regulated, including genes involved in resistance to stress (i.e. adaptation to acidic environment, metabolism, ion homeostasis; Fig 2D, see also S2E, S2G and S2J Fig and S1 Table). In the

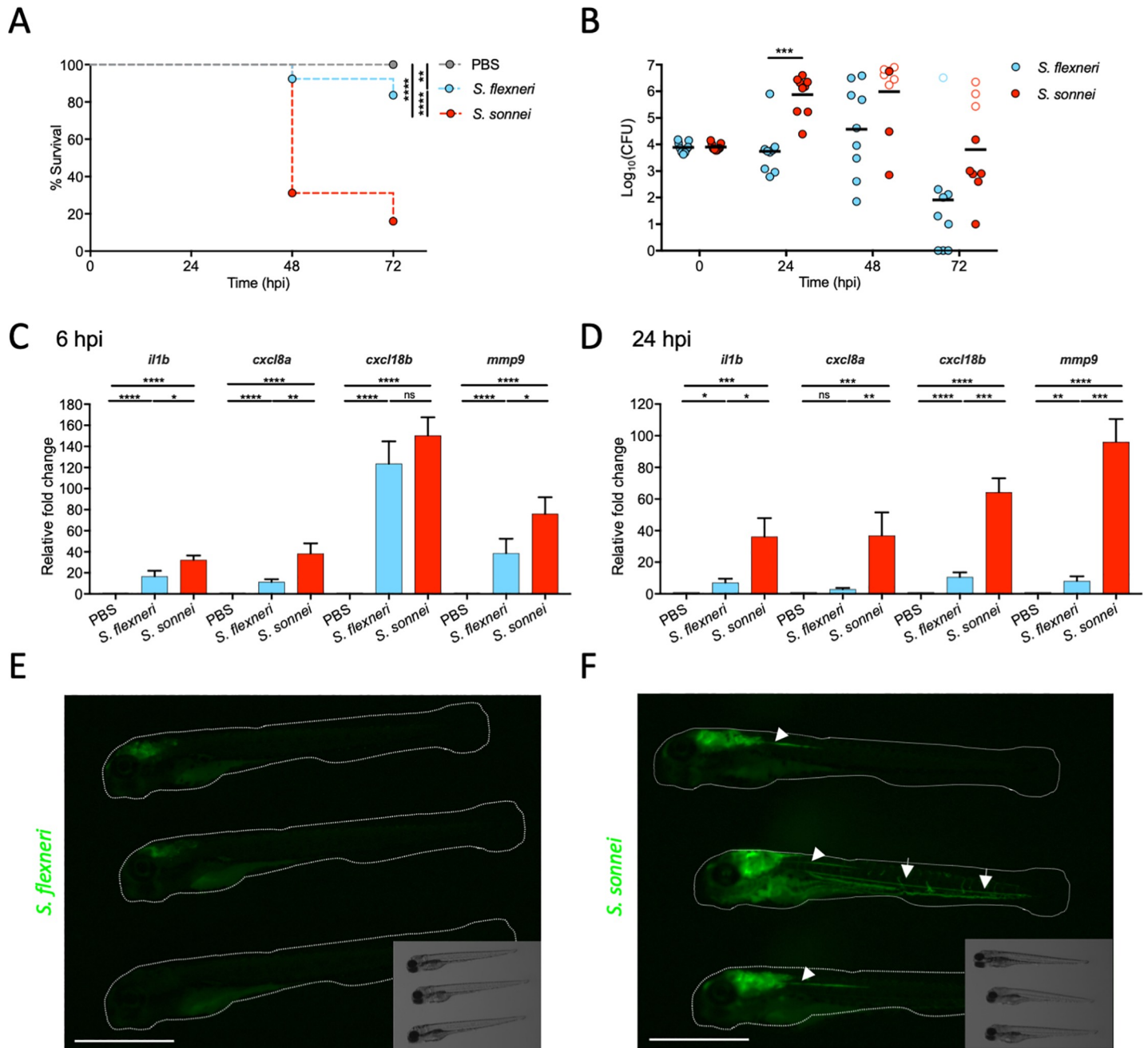
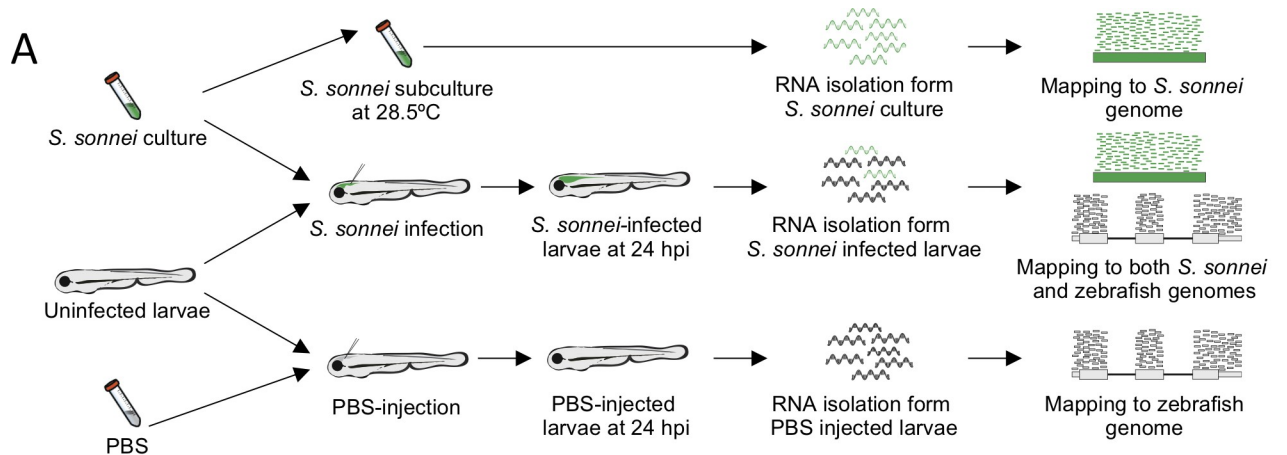


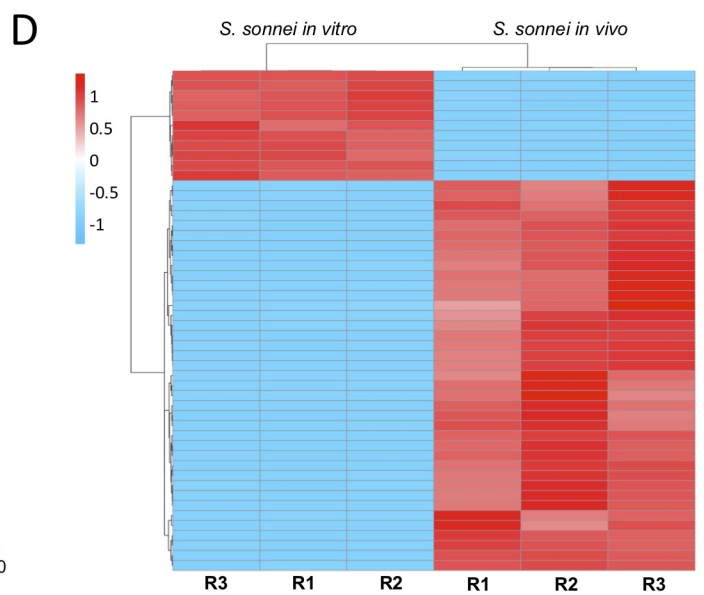
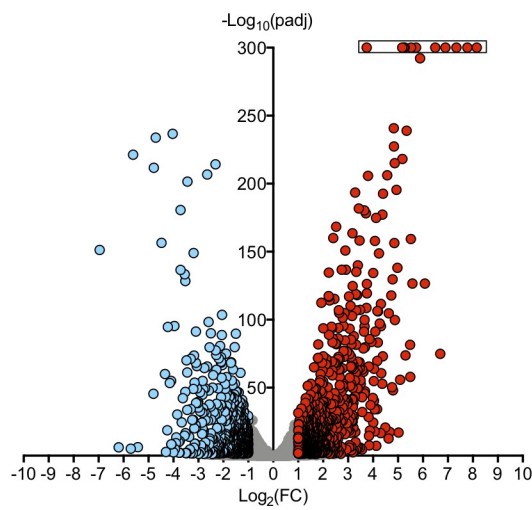
Fig 1. *S. sonnei* is more virulent than *S. flexneri* in a zebrafish infection model. A,B. *S. sonnei* is more virulent than *S. flexneri* *in vivo*. Survival curves (A) and Log₁₀-transformed CFU counts (B) of larvae injected in the hindbrain ventricle (HBV) with PBS (grey), *S. flexneri* (blue) or *S. sonnei* (red). Experiments are cumulative of 3 biological replicates. In B, full symbols represent live larvae and empty symbols represent larvae that at the plating timepoint had died within the last 16 hours. Statistics: Log-rank (Mantel-Cox) test (A); unpaired t-test on Log₁₀-transformed values (B); **p<0.0021; ***p<0.0002; ****p<0.0001. C,D. *S. sonnei* elicits a stronger inflammatory signature than *S. flexneri* *in vivo*. Quantitative real time PCR for representative inflammatory markers were performed on pools of 20 HBV injected larvae collected at 6 (C) or 24 (D) hpi with PBS (grey), *S. flexneri* (blue) or *S. sonnei* (red). Experiments are cumulative of 4 biological replicates. Statistics: one-way ANOVA with Sidak's correction on Log₂-transformed values; ns, non-significant; *p<0.0332 **p<0.0021; ***p<0.0002; ****p<0.0001. E,F. *S. sonnei* can disseminate from the injection site. Representative images of three GFP-labelled *S. flexneri*-infected (E) or *S. sonnei*-infected (F) larvae at 24 hpi. In D, arrows indicate dissemination in the blood circulation; arrowheads indicate dissemination in the neuronal tube. Scale bars = 1 mm.

<https://doi.org/10.1371/journal.ppat.1008006.g001>

case of *S. sonnei*-infected larvae, 283 host genes are significantly upregulated, including inflammatory markers previously tested by qRT-PCR (Fig 1C and 1D) and other genes involved in



B Differentially expressed *S. sonnei* genes



C Differentially expressed zebrafish genes

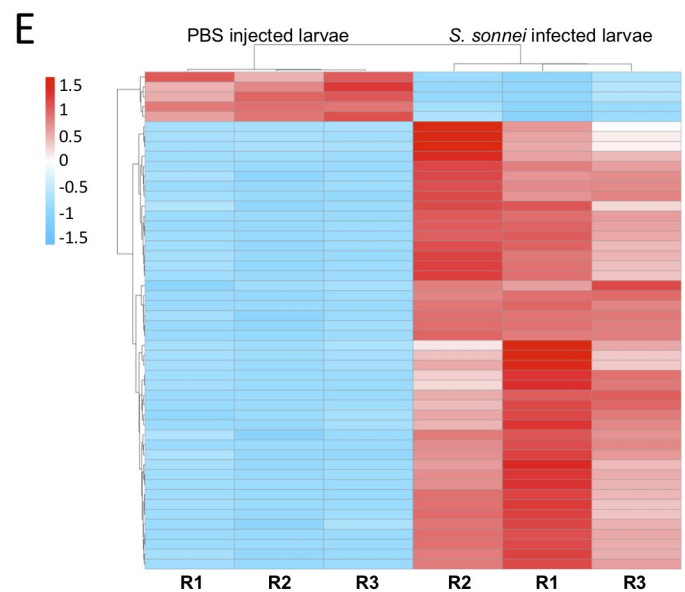
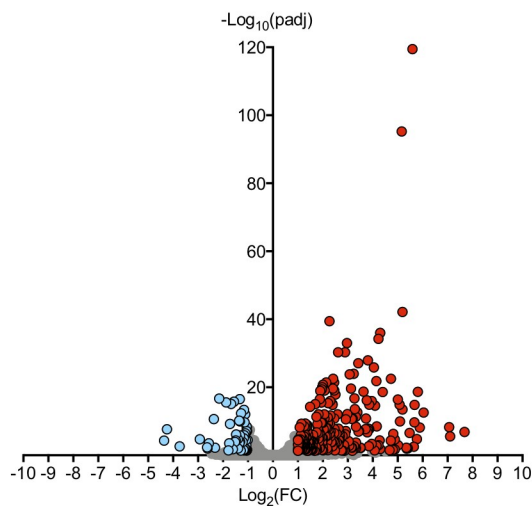


Fig 2. Whole animal dual-RNAseq profiling of *S. sonnei* infected larvae. A. Workflow for dual-RNAseq processing. 3 dpf larvae were infected with ~7000 CFU of *S. sonnei*. Pools of infected larvae were collected for RNA isolation at 24 hpi. As a control for the bacterial transcriptome, the same cultures of *S. sonnei* were diluted 50x and subcultured at 28.5°C (same temperature at which infected larvae are maintained) until Log phase (OD₆₀₀ ~0.6) was reached. As a control for the zebrafish transcriptome, pools of PBS-injected larvae at 24 hpi were used. Reads from infected larvae were mapped separately to both the *S. sonnei* and zebrafish genomes, while reads from *S. sonnei in vitro* cultures and PBS injected larvae were mapped to the pathogen or host genome, respectively. **B,C. Volcano plots for bacterial and zebrafish genes during *S. sonnei* infection.** Each datapoint refers to a single gene. Non significantly differentially expressed genes are shown in grey, while significantly downregulated genes are shown in blue and significantly upregulated genes are shown in red. Plot in B refers to *S. sonnei* genes and plot in C refers to zebrafish genes. See also **S2 Fig** for additional details. Log₂(FC) and -Log₁₀(padj) coordinates were derived from data analysis with the DESeq2 package in R. In B, points enclosed in the black rectangle were computed to have a DESeq2 padj = 0. **D,E. Heatmap of the top 50 differentially expressed bacterial and zebrafish genes during *S. sonnei* infection.** Columns represent individual biological replicates (R1, R2, R3). Heatmaps were created from counts per million (CPM) reads values, using “pheatmap” package in R. Shades of blue indicate downregulation and shades of red indicate upregulation compared to baseline. Plot in D refers to *S. sonnei* genes and plot in E refers to zebrafish genes. From top to bottom, genes represented in D are: adhE_3, glyA, purF, purD, purL, SSON53G_RS25460 (treB-like), gcvP, gcvH, yjiY, gcvT, treC, SSON53G_RS05440 (ymdF-like), gadC, SSON53G_RS20945 (slp-like), otsA, SSON53G_RS02230 (bolA-like), suhB, katE, SSON53G_RS31575 (mcbA-like), hdeD, gadB_1, gadB_2, yohC, gadE, hdeB, SSON53G_RS09595 (narU-like), yegP, ycgB, hdeA, SSON53G_RS20815 (yhiM-like), fadB, yafH, fadA, dadA, artJ, argC, yjgG, argI, yjbJ, aceA, narZ, trxC, aceB_1, argA, modA, ybaT, ybaA, modB, phoH, rmf. From top to bottom, genes represented in E are: krtt1c19e, si:dkey-183i3.5 (thread biopolymer filament subunit alpha-like), zgc:136930 (thread biopolymer filament subunit gamma-like), cyt1, cyt1l, irg1l, si:ch211-153b23.4 (YrdC domain-containing protein-like), si:ch211-153b23.5, timp2b, mmp13a, junbb, tnfaip2b, nox1a, zgc:111983 (mucin-like), c4b, c3a.1, mpeg1.2, si:ch211-39f2.3 (tecta-like), socs3b, tmem176l.4, zgc:174917 (phytanoyl-CoA dioxygenase domain-containing protein 1-like), lgals1l1, cebpb, mmp9, si:ch211-15b10.6 (tifa-like), fosl2, moxd1, cbln11, lect2l, cfb, steap4, irf1b, il1b, si:ch211-183d5.2 (nedd8-like), atf3, cxcl8a, si:dkey-33c14.3 (uncharacterised lincRNA), cxcl18b, cr926130.2 (uncharacterised lincRNA), socs3a, nfkb1a, tnfrsf9a, zgc:153932 (gp2-like), sult5a1, si:dkey-239b22.1 (tecta-like), si:dkey-247k7.2, cr855311.1 (uncharacterised non-coding RNA), cp, cbx7a, c3a.6. Gene names in brackets are inferred by manual annotations based on protein alignments performed on the UniProt database (<https://www.uniprot.org/>). For genes not predicted to encode a protein, manual annotations were inferred from the Ensembl database (<https://www.ensembl.org/>). See also **S1 and S2 Tables** for the extended gene lists and **S2 Fig** for in-depth exploration of the data.

<https://doi.org/10.1371/journal.ppat.1008006.g002>

innate immune signalling, granulopoiesis/neutrophil chemotaxis and inflammation (**Fig 2E**, see also **S2F, S2H, S2I and S2K Fig and S2 Table**). Consistent with this, enrichment analysis for DNA regulatory elements identified the statistical overrepresentation of immune-related transcription factor binding sites (i.e. Rel/Rela, Nfkb2, Stats, Cepbg, Jun, Spi1; **S2 Table**). Together, whole animal dual-RNAseq profiling identified novel markers of *S. sonnei* infection and zebrafish host defence, and we generated an open-access resource for their in-depth exploration. Raw sequencing data are deposited in GEO, the NCBI repository (accession: GSE140544).

S. sonnei virulence depends on its O-antigen

S. sonnei encodes a T6SS and capsule which have been linked to virulence in the murine and rabbit intestine model, respectively (**S3A and S3B Fig**) [18,26]. However, when larvae are infected with a T6SS (*Atssb*) or capsule (*Ag4c*) deficient strain, virulence is not significantly reduced as compared to wildtype (WT) bacteria (**S3C and S3D Fig**). We next infected larvae with a phase II *S. sonnei* strain which lacks the pSS virulence plasmid (-pSS *S. sonnei*). Here, ~100% of larvae survive infection (**Fig 3A and 3B**). Consistent with a role in virulence, the *S. sonnei* pSS plasmid (which is unstable and frequently lost in culture [27]) is retained during zebrafish infection at 28.5°C (**S3E Fig**). The *S. sonnei* pSS encodes a type III secretion system (T3SS) and the biosynthesis machinery for an O-antigen oligosaccharide (O-Ag) non-homologous to those encoded by other *Shigella* species (**S3F Fig**) [28]. Strikingly, infection with O-Ag deficient (Δ O-Ag) *S. sonnei* fully recapitulates results obtained with *S. sonnei* -pSS, while infection with T3SS deficient *S. sonnei* (Δ mxid) demonstrates only partial loss of virulence (**Fig 3A–3D, S3G Fig**). Experiments performed at 32.5°C demonstrate that Δ O-Ag *S. sonnei* remain avirulent at higher temperatures (**S3H–S3K Fig**), and that T3SS-mediated virulence of *S. sonnei* is temperature dependent (**Fig 3A and 3B, S3J and S3K Fig**). Consistent with a role for O-Ag in *S. sonnei* virulence, dual-RNAseq profiling identified *wzzB*/SSON53G_RS12230 (a protein involved in the extension of O-Ag oligosaccharide chains) as significantly upregulated (Log₂(FC) = 1.31, padj = 3.31·10⁻²⁵) during zebrafish infection (**S3L Fig**). To address whether

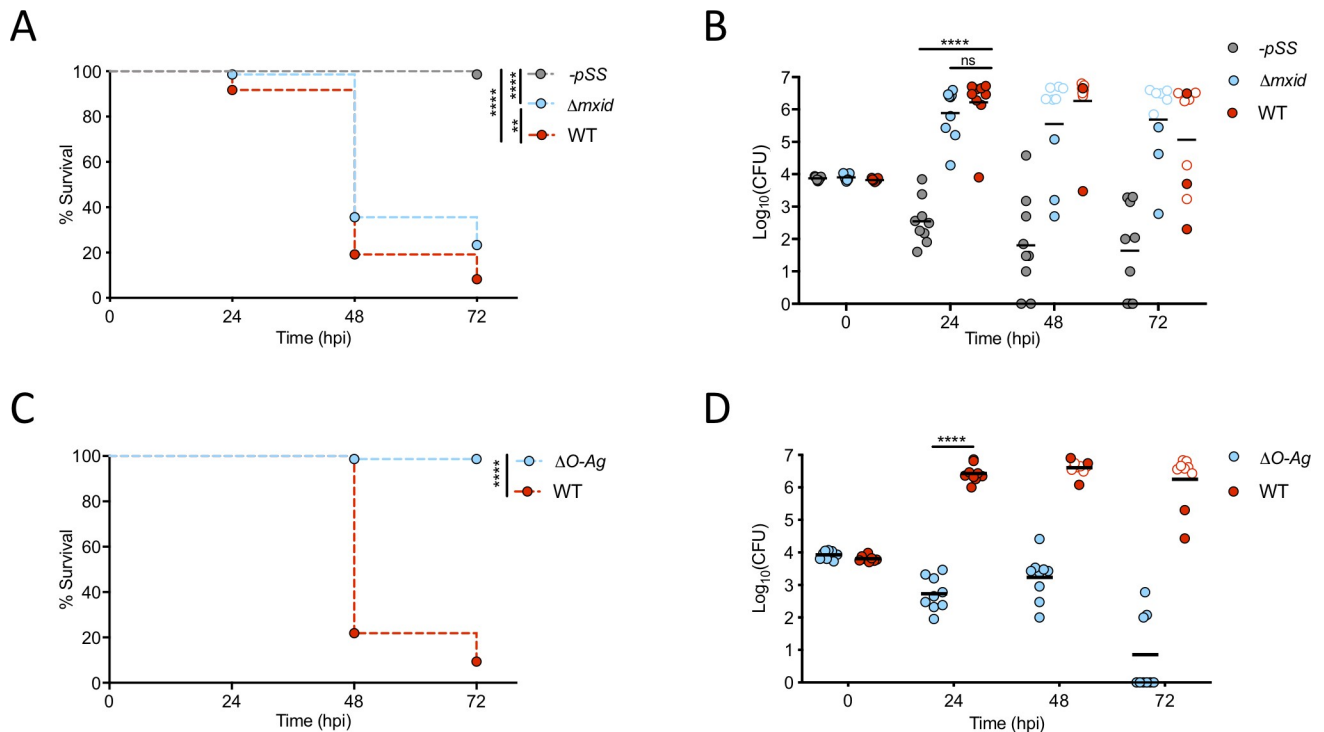


Fig 3. *S. sonnei* virulence depends on its O-antigen. A,B. Virulence of *S. sonnei* depends on its virulence plasmid. Survival curves (A) and Log₁₀-transformed CFU counts (B) of larvae injected in the HBV with *S. sonnei* -pSS (grey), $\Delta mxid$ (blue) or WT (red) strains. Experiments are cumulative of 3 biological replicates. In B, full symbols represent live larvae and empty symbols represent larvae that at the plating timepoint had died within the last 16 hours. Statistics: Log-rank (Mantel-Cox) test (A); one-way ANOVA with Sidak's correction on Log₁₀-transformed data (B); ns, non-significant; ** p < 0.0021; **** p < 0.0001. See also S3H–S3K Fig for experiments at 32.5°C. C,D. Virulence of *S. sonnei* depends on its O-antigen. Survival curves (C) and Log₁₀-transformed CFU counts (D) of larvae injected in the HBV with *S. sonnei* ΔO -Ag (blue) or WT (red) strains. Experiments are cumulative of 3 biological replicates. In D, full symbols represent live larvae and empty symbols represent larvae that at the plating timepoint had died within the last 16 hours. Statistics: Log-rank (Mantel-Cox) test (C); unpaired t-test on Log₁₀-transformed data (D); **** p < 0.0001. See also S3H–S3K Fig for experiments at 32.5°C.

<https://doi.org/10.1371/journal.ppat.1008006.g003>

S. sonnei O-Ag can directly lead to zebrafish death (i.e. due to increased toxicity of the bacterial lipopolysaccharide conjugated with O-Ag), we injected live or heat-killed WT or ΔO -Ag *S. sonnei*. In this case, only live WT *S. sonnei* induced zebrafish death, indicating that *S. sonnei* O-Ag is not toxic *per se* (S3M Fig).

S. sonnei O-antigen can counteract clearance by zebrafish neutrophils

Considering that injection of *S. sonnei* induces recruitment of both macrophages and neutrophils to the HBV at 6 hpi (Fig 4A and 4B), we tested the role of these immune cells in *S. sonnei* virulence. We used the zebrafish line *Tg(mpeg1:Gal4-FF)^{g125}/Tg(UAS-E1b:nfsB.mCherry)^{c264}* in which treatment with the pro-drug Metronidazole (Mtz) results in macrophage ablation (S4A–S4C Fig). Here, the presence or absence of macrophages does not significantly affect zebrafish survival or bacterial burden (Fig 4C and 4D, S4D and S4E Fig). In contrast, when both macrophages and neutrophils are depleted using *pu.1* morpholino oligonucleotide, we observe a significant increase in zebrafish susceptibility to *S. sonnei* (Fig 4E and 4F, S4F–S4H Fig).

Considering an important role for neutrophils in *Shigella* control [22,24], and the significant upregulation of genes involved in granulopoiesis/neutrophil chemotaxis identified by dual-RNAseq profiling (e.g., *cebpb*, *atf3*, *cxcl8a*, *cxcl18b* (Fig 1C and 1D, Fig 2E), we reasoned

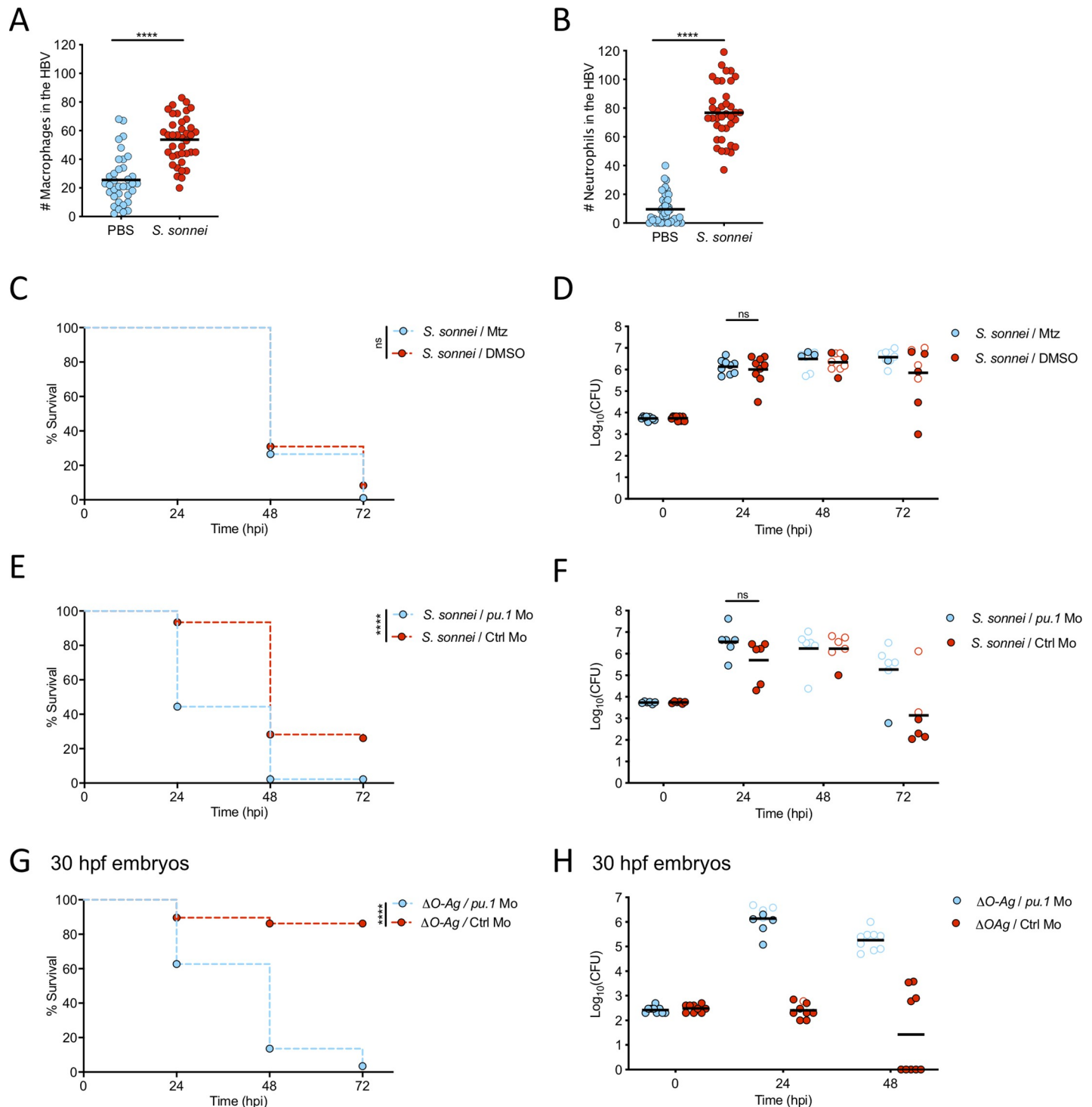


Fig 4. *S. sonnei* O-antigen can counteract clearance by zebrafish neutrophils. A,B. Macrophages and neutrophils are recruited to *S. sonnei* in vivo. Larvae of the *Tg(mpeg1:Gal4-FF)^{g125}/Tg(UAS-E1b:nfsB.mCherry)^{c264}* strain (labelling macrophages, A) or of the *Tg(lyz:dsRed)^{nz50}* strain (labelling neutrophils, B) were injected with PBS (blue) or *S. sonnei* (red) in the HBV. Recruitment was quantified from images at 6 hpi. Experiments are cumulative of 3 biological replicates. Statistics: two-tailed Mann-Whitney test; **** $p < 0.0001$. C,D. Macrophage ablation does not increase susceptibility to *S. sonnei*. Survival curves (C) and Log₁₀-transformed CFU counts (D) of *Tg(mpeg1:Gal4-FF)^{g125}/Tg(UAS-E1b:nfsB.mCherry)^{c264}* larvae which were treated with either Metronidazole (Mtz, macrophage ablated group, blue) or control DMSO vehicle (DMSO, red) prior to infection in the HBV with *S. sonnei*. Experiments are cumulative of 3 biological replicates. In D, full symbols represent live larvae and empty symbols represent larvae that at the plating timepoint had died within the last 16 hours. Statistics: Log-rank (Mantel-Cox) test (C); unpaired t-test on Log₁₀-transformed data (D); ns, non-significant. E,F. *pu.1* morpholino knockdown increases susceptibility to *S. sonnei*. Survival curves (E) and Log₁₀-transformed CFU

counts (F) of *pu.1* morphant (blue) or control (red) larvae infected in the HBV with *S. sonnei*. Experiments are cumulative of 3 biological replicates. In F, full symbols represent live larvae and empty symbols represent larvae that at the plating timepoint had died within the last 16 hours. Statistics: Log-rank (Mantel-Cox) test (E); unpaired t-test on Log₁₀-transformed data (F); ns, non-significant; ****p<0.0001. **G,H. Virulence of Δ O-Ag *S. sonnei* can be observed in *pu.1* morphants.** Survival curves (G) and Log₁₀-transformed CFU counts (H) of *pu.1* morphant (blue) or control (red) larvae infected in the HBV with Δ O-Ag *S. sonnei*. To allow full ablation of immune cells by morpholino knockdown, infections were performed at 30 hours post-fertilisation (hpf). Experiments are cumulative of 3 biological replicates. In H, full symbols represent live larvae and empty symbols represent larvae that at the plating timepoint had died within the last 16 hours. Statistics: Log-rank (Mantel-Cox) test; ****p<0.0001.

<https://doi.org/10.1371/journal.ppat.1008006.g004>

that Δ O-Ag *S. sonnei* may be attenuated *in vivo* because of its inability to counteract neutrophil clearance. Consistent with this hypothesis, infection of *pu.1* morphants at 30 hpf (when depletion of immune cells is complete) with Δ O-Ag *S. sonnei* led to significantly increased zebrafish death, compared to control morphants at the same developmental stage (Fig 4G and 4H, S4I and S4J Fig).

S. sonnei can resist phagolysosome acidification and promote neutrophil cell death in an O-antigen-dependent manner

Using high resolution confocal microscopy, we observed that *S. sonnei* mostly reside within neutrophil phagosomes at 3 hpi (Fig 5A). Additionally, staining of live bacteria with a pH sensitive dye (pHrodo) showed that intracellular *S. sonnei* mostly reside within acidic compartments at 4 hpi (Fig 5B). We therefore hypothesised that O-Ag may promote bacterial survival during phagolysosome acidification. To test this, we measured the growth of WT or Δ O-Ag *S. sonnei* grown in liquid culture at different pH. While the growth of both strains is similar at neutral pH = 7, WT *S. sonnei* grew significantly faster than Δ O-Ag *S. sonnei* at pH = 5 (Fig 5C and 5D, S5A and S5B Fig). Consistent with a role for O-Ag in tolerance to phagolysosome acidification, transmission electron microscopy (TEM) of zebrafish larvae at 3 hpi showed intact and dividing WT *S. sonnei* cells, versus disrupted and non-dividing Δ O-Ag *S. sonnei* cells, in neutrophil phagosomes (Fig 5E and 5F, S5C Fig). Moreover, only in the case of WT *S. sonnei* could we observe compromised nuclei and extranuclear chromatin in zebrafish cells harbouring infection, indicative of necrotic cell death (S5D Fig).

To investigate whether neutrophil cell death mediated by *S. sonnei* is dependent on O-Ag, we quantified neutrophils at the whole animal level in WT or Δ O-Ag *S. sonnei* infected larvae at 6 and 24 hpi. Infection with WT *S. sonnei* resulted in significantly more neutrophil cell death than infection with Δ O-Ag *S. sonnei* (Fig 5G–5J). In the case of *S. flexneri* infection, neutrophils are recognised to die via necrosis [29]. Since no pharmacological reagent exists to directly test necrosis *in vivo*, we sought to rule out other cell death pathways in *S. sonnei* infected larvae and inhibited apoptosis, pyroptosis and/or necroptosis using the pan-caspase inhibitor Q-VD-OPh (an inhibitor of apoptosis and pyroptosis), Necrostatin-1 and/or Necrostatin-5 (inhibitors of necroptosis) (S5E Fig). All inhibitors tested fail to significantly increase zebrafish survival. Considering this, and that infected zebrafish cells appeared necrotic by TEM (S5D Fig), we conclude that neutrophils infected with *S. sonnei* undergo necrosis (and not a programmed mechanism of cell death) because of bacterial survival enabled by *S. sonnei* O-Ag.

Phagolysosome acidification controls S. sonnei clearance by zebrafish and human neutrophils

To test the role of phagolysosome acidification during *S. sonnei* infection *in vivo*, we treated infected larvae with Bafilomycin, an inhibitor of vacuolar H⁺ ATPase (V-ATPase). Consistent with a role for phagolysosome acidification in *S. sonnei* control, Bafilomycin treatment significantly increased zebrafish susceptibility to *S. sonnei* (Fig 6A). Bafilomycin treatment also

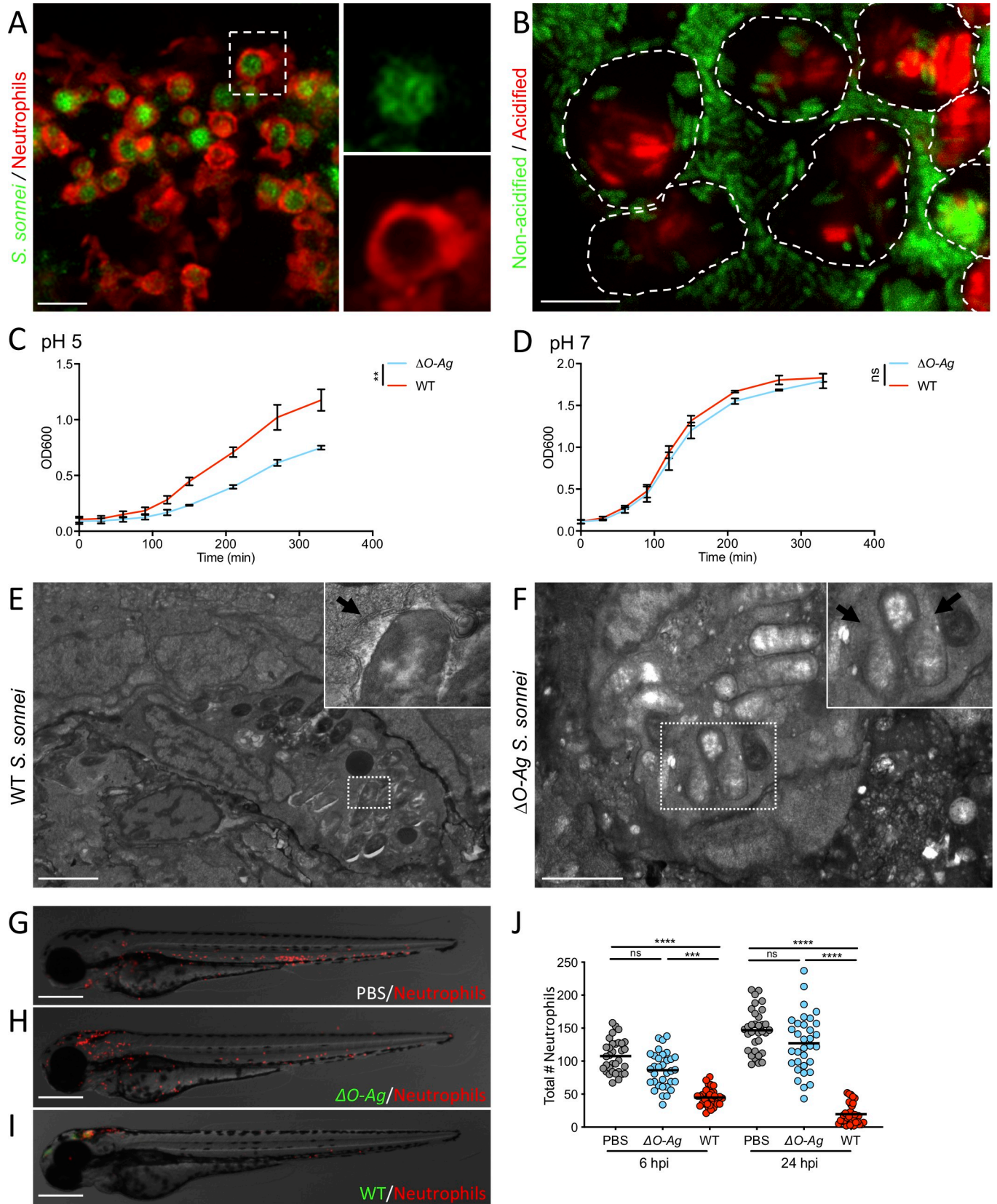


Fig 5. *S. sonnei* can resist phagolysosome acidification and promote neutrophil cell death in an O-antigen-dependent manner. **A. *S. sonnei* is collected by neutrophils in large phagosomes.** Larvae of the *Tg(lyz:dsRed)^{nz50}* strain (labelling neutrophils) were injected in the HBV with WT GFP-*S. sonnei*. Image taken at 3 hpi. Scale bar = 20 μ m. **B. *S. sonnei* is acidified in immune cell phagosomes.** Larvae were injected in the HBV with WT GFP-*S. sonnei* which was also stained with pHrodo, a pH-sensitive dye that turns red in acidic environments. Image taken at 4 hpi, where GFP signal is attenuated for bacteria residing in acidified phagosomes (i.e. GFP is unstable and quenched at pH<6). Dashed lines highlight the outline of individual phagocytes. Scale bar = 10 μ m. **C,D. *S. sonnei* O-antigen contributes to acid tolerance in vitro.** Growth curves of Δ O-Ag (blue) or WT (red) *S. sonnei*, cultured in tryptic soy broth adjusted to pH = 5 (C) or 7 (D). Statistics: unpaired t-test at the latest timepoint; ns, non-significant; **p<0.0021. **E,F. *S. sonnei* requires the O-antigen to survive in phagosomes.** Transmission electron micrographs of infected phagocytes from zebrafish larvae at 3 hpi with WT (E) or with Δ O-Ag (F) *S. sonnei*. E shows an intact phagocyte and *S. sonnei* residing within a phagosome (arrow points at phagosomal membrane). F shows that Δ O-Ag *S. sonnei* bacteria being degraded by a phagocyte (arrows point at region of major loss of bacterial cell integrity). Scale bars = 3 μ m (E); 2 μ m (F). **G-J. The O-antigen is required for *S. sonnei*-mediated killing of neutrophils.** Representative micrographs of larvae of the *Tg(lyz:dsRed)^{nz50}* strain injected in the HBV with PBS (G), GFP- Δ O-Ag (H) or WT (I) *S. sonnei* at 6 hpi and quantification of total neutrophil number at 6 and 24 hpi (J). Statistics: Kruskal-Wallis test with Dunn's correction; ns, non-significant; ****p<0.0001. Scale bars = 250 μ m.

<https://doi.org/10.1371/journal.ppat.1008006.g005>

increased zebrafish susceptibility to Δ O-Ag *S. sonnei* (Fig 6B), highlighting the virulence of Δ O-Ag *S. sonnei* in the absence of phagolysosome acidification.

Considering that inhibition of phagolysosome acidification increases zebrafish susceptibility to *S. sonnei*, we hypothesised that promotion of acidification may overcome tolerance provided by O-Ag *in vivo*. V-ATPases mediate phagolysosome acidification by using ATP to pump protons in acidifying compartments. Injections of 200 μ M ATP 3 h prior to *S. sonnei* infection significantly increases zebrafish survival (Fig 6C). Bafilomycin directly antagonises V-ATPase activity. In agreement with this, treatment of *S. sonnei* infected larvae with Bafilomycin counteracts the beneficial effects of ATP injection for host defence (Fig 6D).

To test the role of *S. sonnei* O-Ag in human infection, we isolated peripheral neutrophils from healthy donors and infected them with WT or Δ O-Ag *S. sonnei* (Fig 6E). In agreement with results from zebrafish infection, Δ O-Ag *S. sonnei* are significantly more susceptible to human neutrophil-mediated clearance than WT bacteria, and Bafilomycin treatment increased susceptibility of human neutrophils to Δ O-Ag *S. sonnei* (Fig 6F). Plasmid reintroduction of the O-Ag biosynthesis system in Δ O-Ag *S. sonnei* (Δ O-Ag^{+pSSO-Ag}) could restore the resistance of mutant bacteria to neutrophil killing to levels observed using WT bacteria (Fig 6E and 6F; S3G Fig). Collectively, these results show that *S. sonnei* O-Ag enables neutrophil tolerance in zebrafish and human neutrophils, and suggest that promotion of phagolysosome acidification is a novel approach to counteract *S. sonnei* infection (Fig 6G and 6H).

The innate immune system can be trained to control *S. sonnei* *in vivo*

Neutrophils of zebrafish larvae can be trained to protect against *S. flexneri* infection [25]. To test if we can enhance innate immunity to *S. sonnei*, we developed a *S. sonnei* reinfection assay (Fig 7A). For this, larvae at 2 dpf were injected in the HBV with PBS or a sublethal dose (~80 CFU) of WT or Δ O-Ag GFP-*S. sonnei*. At 48 hpi, we screened larvae and found that ~20% of WT *S. sonnei* infected larvae are unable to clear infection (S6A and S6B Fig); these larvae were therefore excluded from further analysis. Next, PBS-injected larvae or larvae clearing the primary infection (as determined by fluorescence microscopy) were infected with a lethal dose (~8000 CFU) of mCherry-*S. sonnei*. Strikingly, injection of larvae with WT *S. sonnei* (but not Δ O-Ag *S. sonnei*) significantly increased survival, as compared to PBS-injected larvae (Fig 7B and 7C). These experiments show that larvae exposed to a sublethal dose of *S. sonnei* are protected against a secondary lethal dose of *S. sonnei* in an O-Ag-dependent manner, and may have important implications in vaccine design.

Discussion

Why *S. sonnei* is emerging globally as a primary agent of bacillary dysentery has been unknown. Here, we discover that *S. sonnei* is more virulent than *S. flexneri* *in vivo* because of

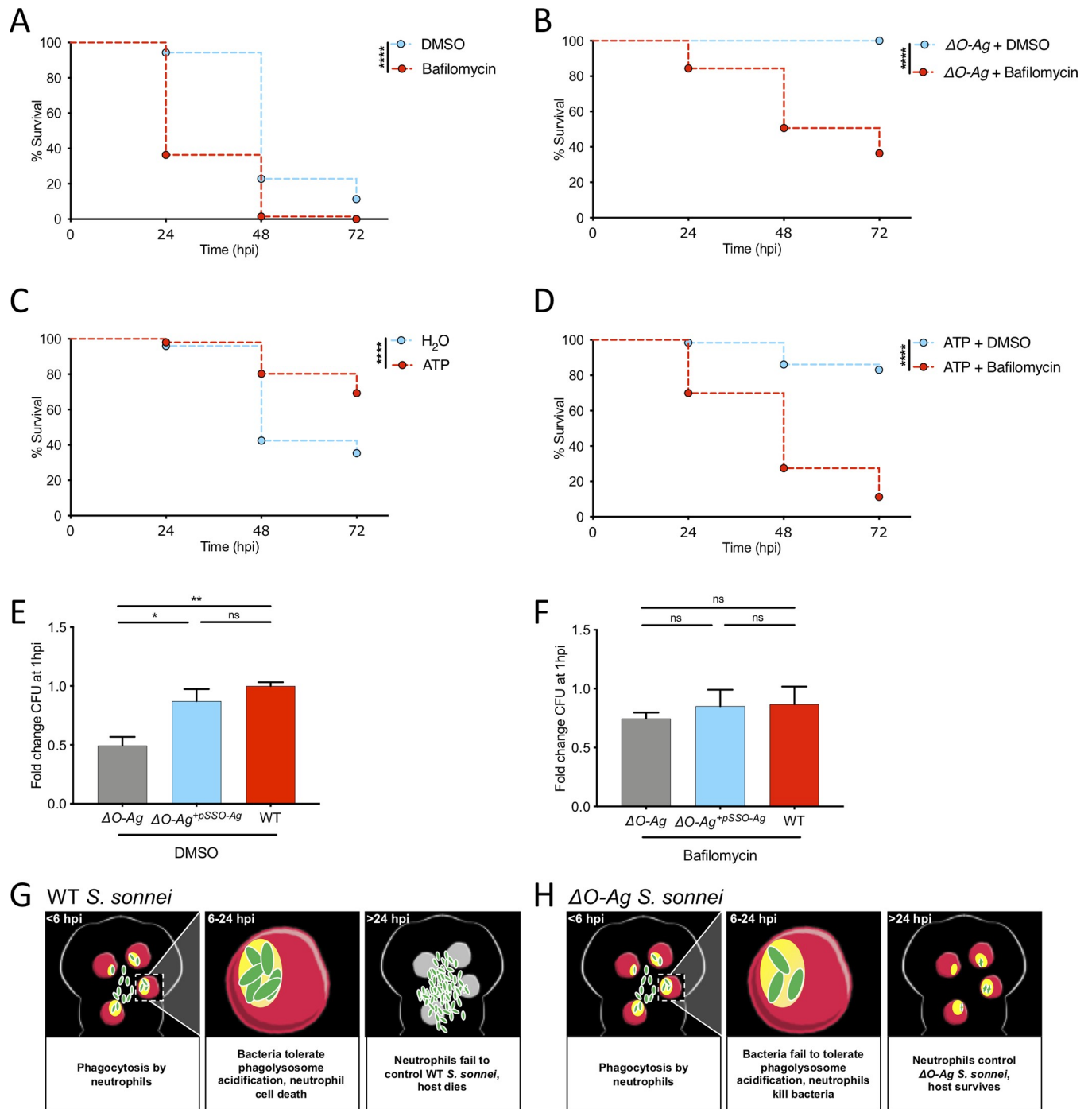


Fig 6. Phagolysosome acidification controls *S. sonnei* clearance by zebrafish and human neutrophils. A,B. Bafilomycin treatment increases susceptibility to WT and ΔO -Ag *S. sonnei*. Survival curves of larvae treated with control DMSO vehicle (blue) or Bafilomycin (red) upon infection in the HBV with WT (A) or ΔO -Ag (B) *S. sonnei*. Experiments are cumulative of 3 biological replicates. Bacterial input: ~7000 CFU. Statistics: Log-rank (Mantel-Cox) test; ****p<0.0001. C. ATP injections protect against *S. sonnei* infection. Survival curves of larvae injected in the HBV with control water (blue) or ATP (red) 3 hours prior to infection of the same compartment with *S. sonnei*. Experiments are cumulative of 3 biological replicates. Bacterial input: ~7000 CFU. Statistics: Log-rank (Mantel-Cox) test; ****p<0.0001. D. Bafilomycin treatment and ATP injections counteract each other. Survival curves of larvae injected in the HBV with ATP 3 hours prior to infection of the same compartment with *S. sonnei* and treatment with control DMSO vehicle (blue) or Bafilomycin (red). Experiments are cumulative of 3 biological replicates. Bacterial input: ~7000 CFU. Statistics: Log-rank (Mantel-Cox) test; ****p<0.0001. E,F. *S. sonnei* O-Ag is required to counteract acidification-mediated clearance by human neutrophils. ΔO -Ag (grey), complemented strain (ΔO -Ag^{+pSSO-Ag}, blue) or WT (red) *S. sonnei* were incubated with peripheral human neutrophils and exposed to DMSO (vehicle control treatment, E) or Bafilomycin (F). Difference in bacterial killing was quantified by plating from lysates of infected neutrophils at 1 hpi. Experiments are cumulative of 3 biological replicates from 3 independent donors. Statistics:

one-way ANOVA with Sidak's correction; ns, non-significant; * $p < 0.0332$; ** $p < 0.0021$. **G,H. Model of *S. sonnei* O-antigen counteracting neutrophils *in vivo*.** Upon phagocytosis of WT *S. sonnei* (green), zebrafish neutrophils (red) rapidly acidify phagolysosomes containing bacteria. However, *S. sonnei* can tolerate this environment because of its O-antigen. *S. sonnei* replication leads to neutrophil and host death (G). *S. sonnei* without O-antigen fails to counteract acidification of neutrophil phagolysosomes. In this case, neutrophils clear infection and the host survives (H).

<https://doi.org/10.1371/journal.ppat.1008006.g006>

neutrophil tolerance mediated by its O-Ag. We also show that increased phagolysosomal acidification or innate immune training can promote *S. sonnei* clearance by neutrophils *in vivo* and propose new approaches to *S. sonnei* control.

The O-Ag, a lipopolysaccharide component of Gram-negative bacteria consisting of repetitive surface oligosaccharide units, is a major target for the immune system and bacteriophages. As a result, it is viewed that co-evolution of bacteria with their hosts or phages has led to significant variation in O-Ag structure/composition across bacterial strains [30]. In the case of most *Shigella spp.*, significant variation of their *E. coli*-like O-Ag is observed across strains [28]. Interestingly, genes involved in *S. sonnei* O-Ag biosynthesis are non-homologous to those of other *Shigella spp.*, highly conserved across *S. sonnei* strains and the only example of a virulence-plasmid encoded O-Ag system (in other *Shigella spp.* the O-Ag is encoded by

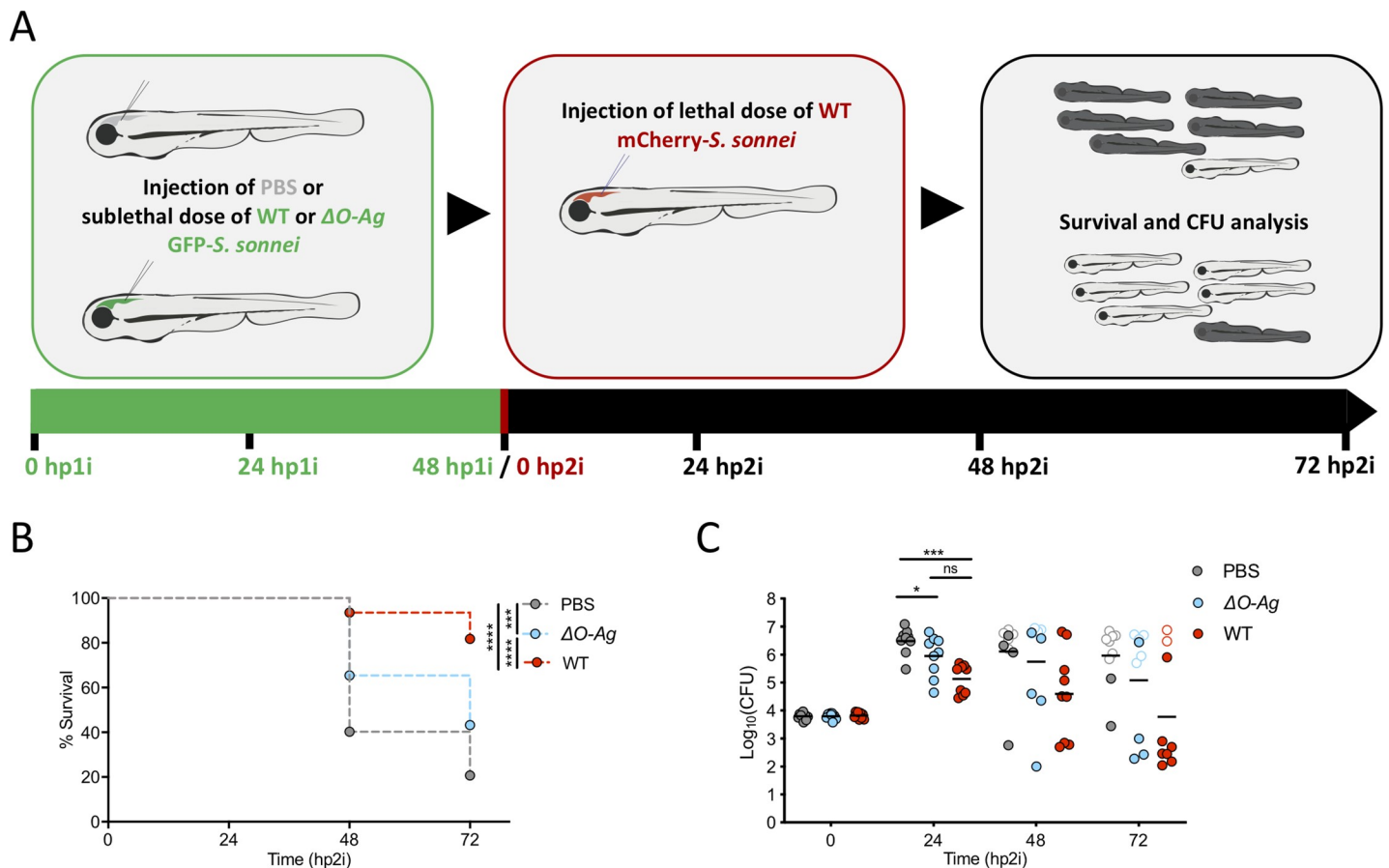


Fig 7. Innate immunity can be trained to control *S. sonnei* *in vivo*. **A. Model for *S. sonnei* reinfection.** 2 dpf embryos were primed with PBS or a sublethal dose of *S. sonnei*. At 48 hours post primary infection (hp1i), larvae were challenged with a lethal dose of *S. sonnei* and monitored by survival assay for 72 hours post-secondary infection (hp2i). **B,C. Innate immune training to *S. sonnei* is dependent on O-antigen.** Survival curves (B) and Log_{10} -transformed CFU counts (C) of 4 dpf larvae infected in the HBV with lethal dose (~8000 CFU) of mCherry-WT *S. sonnei*. 48 hours prior to infection with lethal dose, embryos were primed by delivering PBS (grey), or a sublethal dose (~80 CFU) of GFP- Δ O-Ag (blue) or GFP-WT (red) *S. sonnei*. Experiments are cumulative of 4 (B) or 3 (C) biological replicates. In C, full symbols represent live larvae and empty symbols represent larvae that at the plating timepoint had died within the last 16 hours. Statistics: Log-rank (Mantel-Cox) test (B); one-way ANOVA with Sidak's correction on Log_{10} -transformed data (C); ns, non-significant; * $p < 0.0332$; ** $p < 0.0002$; **** $p < 0.0001$.

<https://doi.org/10.1371/journal.ppat.1008006.g007>

chromosomal genes) [28]. Consistent with this, acquisition of O-Ag genes from *P. shigelloides* is considered a defining event for the emergence of *S. sonnei* [16,31]. We show that *S. sonnei* O-Ag enables bacteria to resist phagolysosome acidification and promotes neutrophil cell death. In agreement with this, chemical inhibition or promotion of phagolysosome acidification respectively decreases and increases neutrophil control of *S. sonnei* and zebrafish survival. In future studies it will be important to investigate the precise role of *S. sonnei* O-Ag in tolerance to phagolysosome acidification in neutrophils, and inspire new approaches for *S. sonnei* control.

Innate immune memory is a primitive form of immune memory conserved across vertebrates [32,33]. We reveal that larvae injected with a sublethal dose of *S. sonnei* are protected against a secondary lethal dose of *S. sonnei* in an O-Ag-dependent manner. Although there is no vaccine currently available for *S. sonnei*, our results suggest that training innate immune memory against O-Ag should be considered for vaccine development. Moreover, it is tempting to speculate that innate immune memory may help to explain the increasing *S. sonnei* burden in regions where improved water sanitation has eliminated *P. shigelloides* and subsequently reduced cross-immunisation against *S. sonnei* O-Ag [16,17]. Consistent with this, the incidence of *S. sonnei* infection is mostly observed in very young children (<5 years old) [34–38], an age group where trained innate immunity has been shown to play an important protective role [32,33,39–41].

Collectively, these findings reveal O-antigen as an important therapeutic target against bacillary dysentery. These findings also have major implications for our evolutionary understanding of *Shigella* and may explain the increasing burden of *S. sonnei* in developing countries.

Materials and methods

Ethics statements

Animal experiments were performed according to the Animals (Scientific Procedures) Act 1986 and approved by the Home Office (Project licenses: PPL P84A89400 and P4E664E3C). All experiments were conducted up to 7 days post fertilisation.

Tissue samples from anonymised human donors (neutrophils) were provided by the Imperial College Healthcare NHS Trust Tissue Bank 12275. Other investigators may have received samples from these same tissues.

Zebrafish

Zebrafish lines used here were the wildtype (WT) AB strain, macrophage reporter line *Tg(mpeg1:Gal4-FF)^{g125}/Tg(UAS-E1b:nfsB.mCherry)^{c264}* and neutrophil reporter line *Tg(lyz:dsRed)^{nz50}*. Unless specified otherwise, eggs, embryos and larvae were reared at 28.5°C in Petri dishes containing embryo medium, consisting of 0.5x E2 water supplemented with 0.3 µg/ml methylene blue (Sigma-Aldrich, St. Louis, Missouri). For injections and *in vivo* imaging, anaesthesia was obtained with buffered 200 µg/ml tricaine (Sigma-Aldrich) in embryo medium. Protocols are in compliance with standard procedures as reported at zfin.org.

Bacterial preparation and infection delivery

Unless specified otherwise, GFP fluorescent or non-fluorescent *S. flexneri* M90T or *S. sonnei* 53G were used. Mutant, transgenic and WT strains are as indicated in the Figure legends and further detailed in [S3 Table](#).

Bacteria were grown on trypticase soy agar (TSA, Sigma-Aldrich) plates containing 0.01% Congo red (Sigma-Aldrich) supplemented, when appropriate, with antibiotics (Carbenicillin 100 µg/ml (Sigma-Aldrich), Kanamycin 50 µg/ml (Sigma-Aldrich), Streptomycin 50 µg/ml (Sigma-Aldrich)). Individual colonies were selected and grown O/N, 37°C/200 rpm, in 5 ml trypticase soy broth (TSB, Sigma-Aldrich) supplemented with the appropriate antibiotics as above. For injections, bacteria were grown to Log phase by diluting 400 µl of O/N culture in 20 ml of fresh TSB (supplemented, where appropriate, with 25 µg/ml Carbenicillin) and culturing as above until an optical density (OD) of 0.55–0.65 at 600 nm.

Bacteria were spun down, washed in phosphate buffer saline (PBS, Sigma-Aldrich) and resuspended at the desired concentration in a final injection buffer containing 2% polyvinylpyrrolidone (Sigma-Aldrich) and 0.5% phenol red (Sigma-Aldrich) in PBS (injection buffer alone is referred into the text as PBS group). Heat-killed bacteria were prepared as described above, but the bacterial inoculum was incubated for 30 min at 60°C prior to injection.

Unless specified otherwise, 1–2 nl of bacterial suspension (bacterial load as indicated in the individual experiments) or control solution were microinjected in the hindbrain ventricle (HBV) of 3 days post-fertilisation (dpf) zebrafish larvae (or at 2 dpf followed by reinfection at 4 dpf for reinfection assays, **Fig 7B and 7C**). In **S1G and S1H Fig** infection was delivered intravenously (IV), via the Duct of Cuvier.

Bacterial enumeration was performed *a posteriori* by mechanical disruption of infected larvae in 0.4% Triton X-100 (Sigma-Aldrich) and plating of serial dilutions onto Congo red-TSA plates.

The *S. sonnei* 53G $\Delta tssB$ strain was created using the λ Red recombinase approach [42]. Briefly, the *aphA-3* cassette encoding Kanamycin resistance with flanking extensions homologous to the upstream and downstream regions of *tssB* was created by overlapping PCR using primers #1 and #2 (upstream *tssB*), #3 and #4 (downstream *tssB*) and #5 and #6 (Kan^R). Primer sequences are reported in **S4 Table**. The linear fragment was amplified (primers #1 and #4), parental plasmid removed by DpnI digestion and the linear fragment gel purified. The linear fragment was transformed into electrocompetent *S. sonnei* 53G containing pKD46; the λ Red recombinase genes on this plasmid were induced by arabinose prior to transformation. $\Delta tssB$ colonies were selected on Kanamycin plates, and gene disruption was verified by multiple PCRs (primers #7 and #8, #6 and #8). pKD46 loss was confirmed by Ampicillin sensitivity. Successful gene disruption was also confirmed by sequencing of the entire region using primers #7 and #8.

The *S. sonnei* 53G ΔO -Ag and its complemented strain ΔO -Ag^{+pSSO-Ag} are described in [43]. Briefly, the O-Ag synthesis operon *wbgT-wbgZ* was replaced by a Kanamycin cassette using the λ Red recombinase approach as described above. This mutant was complemented *in trans* with the entire O-Ag synthesis operon (including the upstream chain length regulator *wzz* and 102 bp 5' of *wzz* and 76 bp 3' of *wbgZ* to include endogenous transcriptional promoters and terminators) inserted into a low copy number vector pSEVA421:SmR. To validate strains, crude LPS was isolated from ~5 ml O/N cultures (~16 h) equalised by optical density. The LPS preparation was run on a 12% SDS-PAGE gel and blotted using an anti-*S. sonnei* Phase I antibody (ab78678, Abcam, Cambridge, UK).

To quantify the loss of virulence plasmid (**S3E Fig**) GFP-labelled bacteria were injected in zebrafish larvae (1 nl, ~7000 CFU/nl) as above or spotted onto Congo red-TSA plates (10 µl, ~7000 CFU/nl). Larvae and plates were incubated at 28.5°C for 24 h, bacteria were harvested from plates or larvae, and plated in serial dilutions on Carbenicillin-supplemented plates, grown O/N at 37°C and quantified for loss of virulence plasmid (white versus red colonies) as described elsewhere [27].

To address sensitivity of bacterial strains to acidic pH (Fig 5C and 5D, S5A and S5B Fig), bacteria were first grown O/N as described above, diluted to the same initial OD₆₀₀ (0.10) in pH-adjusted TSB and bacterial growth was monitored by OD₆₀₀ measurements at different timepoints. The pH of TSB was adjusted by addition of few drops of concentrated HCl (Sigma-Aldrich).

Infection of human neutrophils

At least 5 ml of peripheral blood was drawn from healthy volunteers, using EDTA as an anticoagulant (BD Vacutainer, Becton Dickinson, Franklin Lakes, New Jersey). Neutrophils were isolated by gradient centrifugation using Polymorphprep™ (Axis-Shield, Dundee, UK), according to the manufacturer's guidelines and previously described protocols [44]. Residual erythrocytes were removed by incubation for 10 minutes at 37°C in erythrocyte lysis buffer, consisting of 0.83% w/v NH₄Cl (Sigma-Aldrich), 10 mM NaOH-buffered HEPES (4-(2-hydroxyethyl)-1-piperazineethanesulfonic acid, Sigma-Aldrich), pH 7.4. Purified neutrophils were washed in Hank's Balanced Salt Solution (HBSS) without Calcium and Magnesium (HBSS -Ca²⁺/-Mg²⁺, Thermo Fisher Scientific, Waltham, Massachusetts), resuspended in neutrophil medium, consisting of HBSS with Calcium and Magnesium (HBSS +Ca²⁺/+Mg²⁺, Thermo Fisher Scientific) and 0.1% porcine gelatin (Sigma-Aldrich), counted using trypan blue staining, and ultimately diluted at a density of 2 x 10⁶ live cells/ml in neutrophil medium [44]. Prior receiving infection, 10⁵ neutrophils (50 µl of neutrophil resuspension) were pre-incubated with Bafilomycin (111,11 nM, Sigma-Aldrich) [45,46] or DMSO at vehicle control levels for 30 minutes with gentle shaking at 37°C in 48-well plates and in a total volume of 180 µl of neutrophil medium.

For neutrophil infections, *Shigella* was cultured as described above, but ultimately resuspended in neutrophil medium at a density of 5 x 10⁴ CFU/ml and 10³ bacteria (20 µl of bacterial resuspension) were added to the neutrophil resuspension and incubated for 1 h with gentle shaking at 37°C. Neutrophils were lysed by incubation on ice and addition of 7.5 µl of 0.4% Triton X-100 (Sigma-Aldrich) per well. Total CFUs were calculated by plating 20 µl of the lysate, comparing infected neutrophil samples to control samples, lacking neutrophils [44].

pHrodo staining

pHrodo Red, succinimidyl ester (Thermo Fisher Scientific) was prepared according to the manufacturer's guidelines. 0.25 µl of stock solution were used to stain 200 µl of a ~7000 CFU/nl bacterial suspension in PBS. Bacteria were incubated in the dark at 28.5°C for 30 minutes, washed 3 times in PBS, resuspended in 2% polyvinylpyrrolidone and 0.5% phenol red in PBS and injected in the HBV as above.

Light and electron microscopy imaging

Stereo fluorescent microscopy images were acquired using Leica M205FA stereo fluorescent microscopes (Leica, Wetzlar, Germany). Zebrafish larvae were anaesthetised and aligned on 1% agarose plates in embryo medium.

For high-resolution confocal microscopy, imaging was performed using a Zeiss LSM 880 (Carl Zeiss, Oberkochen, Germany). Larvae were positioned in 35-mm-diameter glass-bottom MatTek dishes and imaged with 20× air or 40× water immersion objectives. Image files were processed using ImageJ/FIJI software.

For electron microscopy analysis, infected zebrafish larvae and controls were fixed at 3 hpi in 0.5% glutaraldehyde/200 nM sodium cacodylate buffer for 2 h and washed in cacodylate buffer only. Samples were then fixed in reduced 1% osmium tetroxide/1.5% potassium

ferricyanide for 60 min, washed in distilled water and stained overnight at 4°C in 0.5% magnesium uranyl acetate. Specimens were then washed in distilled water, dehydrated in graded ethanol, infiltrated with propylene oxide and then graded Epon/PO mixtures until final embedding in full Epon resin in coffin moulds. Resin was allowed to polymerise at 56°C overnight, then semi-thin survey sections were cut and stained. Final ultrathin sections (typically 50–70 nm) and serial sections were collected on Formvar coated slot grids, stained with Reynolds's lead citrate and examined in a FEI Tecnai electron microscope with CCD camera image acquisition system.

qRT-PCR

qRT-PCRs were performed using StepOne Plus machine (Applied Biosystems, Foster City, California) and a SYBR green master mix (Applied Biosystems). Briefly, RNA was isolated from pools of whole larvae using RNeasy mini kit (Qiagen, Hilden, Germany). cDNA was obtained using a QuantiTect reverse transcription kit (Qiagen). Samples were run in technical duplicates and quantification was obtained using the $2^{-\Delta\Delta CT}$ method and *eef1a1a* as a house-keeping gene. [S4 Table](#) reports all primers used in this study.

Enumeration of immune cells

For recruitment assays, immune cells attracted to the infection site were enumerated from images by counting *Tg(mpeg1:Gal4-FF)^{g125}/Tg(UAS-E1b:nfsB.mCherry)^{c264}* (for macrophages) or *Tg(lyz:dsRed)^{nz50}* (for neutrophils) positive cells in the hindbrain/midbrain. To quantify neutrophil death, the same neutrophil line was used to count immune cells at the whole animal level.

Chemical treatments, ablations and knockdowns in zebrafish

Macrophages were ablated by exposing hatched 2 dpf *Tg(mpeg1:Gal4-FF)^{g125}/Tg(UAS-E1b:nfsB.mCherry)^{c264}* embryos to Metronidazole (Mtz, Sigma-Aldrich) at 100 μM concentration in 1% DMSO (Sigma-Aldrich) for 24 h [47]. Treatment with 1% DMSO alone was used as a control.

Morpholinos were purchased from Gene Tools (Philomath, Oregon). Injections of *pu.1* (*spi1ab*) morpholino (2 nl, 0.5 mM in 0.5% phenol red) were performed at 1-cell stage and the same volume and concentration of a standard control morpholino was used as negative control. Morpholino sequences are reported in [S4 Table](#).

Necrostatin-1 (10 μM, Santa Cruz Biotechnology, Dallas, Texas), Necrostatin-5 (10 μM, Santa Cruz) [48], Q-VD-OPh (50 μM, Sigma-Aldrich) [49] and Bafilomycin (200 nM, Sigma-Aldrich) [45,50] were provided by bath exposure from 0 hpi for the whole infection course. Exposure to DMSO at vehicle concentration (0.67% for Necrostatin-1, Necrostatin-5, Q-VD-OPh, and 0.2% for Bafilomycin) was used as a control. Priming with ATP injections was performed by injecting 1 nl of 200 mM ATP in the hindbrain 3 h prior infection. Injection of 1 nl of sterile water was used as a vehicle control.

Dual-RNAseq sample preparation and analysis

RNA samples for dual-RNAseq were extracted in triplicate from infected larvae at 24 hpi using 24 larvae/sample. As a control for the host transcriptome, RNA was isolated from corresponding PBS injected larvae at the same timepoint. As a control for *S. sonnei* transcriptome, RNA was isolated from the same culture used for injection, but diluted 50x and subcultured at 28.5°C until it reached the OD of ~0.6 in a total volume of 5 ml. Samples were snap frozen at

-80°C, then 100 µl of RNA protect bacteria reagent (Qiagen) was added, followed by mechanical trituration with a pestle blender. Samples were supplemented with 100 µl of 30 mM Tris-HCl/1 mM EDTA solution at pH = 8, 33 µl of 50 mg/ml lysozyme (Thermo Fisher Scientific), 33 µl of proteinase K >600 U/ml (Thermo Fisher Scientific) and shaken for 20 min RT. Lysis was completed by adding 700 µl of RTL buffer (Qiagen), 3 µl of 1 M dithiothreitol (Sigma-Aldrich) and mechanical disruption. Undigested debris were spun down 3 min 10000 rpm and the supernatant was supplemented with 500 µl of 100% ethanol prior loading onto RNeasy mini columns (Qiagen). From this step onwards, the manufacturer's guidelines were followed for RNA purification. RNA quality and integrity were assessed by using NanoDrop and Non-denaturing agarose gel electrophoresis. For further quality check, RNA sequencing, library construction and reads count, samples were outsourced to Vertis Biotechnologie AG (Freising, Germany). Bacterial and host mRNA were enriched prior library preparation by using Ribo-Zero Gold rRNA Removal Kit (Epidemiology, Illumina, San Diego, California). The zebrafish genome assembly GRCz11 (http://www.ensembl.org/Danio_rerio) and the *S. sonnei* 53G genome assembly ASM28371v1 (<https://www.ncbi.nlm.nih.gov/assembly/406998>) were used to guide mapping of host and pathogen reads, respectively. The average library depths for the different sample groups were: 8658688 +/- 598491 reads (PBS injected larvae), 7771779 +/- 804881 reads (infected larvae), 11315345 +/- 551602 reads (*S. sonnei in vitro*) and 702385 +/- 12785 reads (*S. sonnei in vivo*).

RNAseq statistical analysis was performed using DESeq2 package in R [51,52]. Genes that were not represented with at least 6 reads cumulative from all samples were excluded from the analysis *a priori*. Genes were accepted as differentially expressed if the DESeq2 Log₂(Fold Change) > |1| and DESeq2 adjusted p value (padj) < 0.05. Heatmaps (Fig 2D and 2E) were obtained from counts per million (CPM) reads using the "pheatmap" package (<https://CRAN.R-project.org/package=pheatmap>). Principal component analysis (PCA) (S2A and S2B Fig) was also performed in R from CPM reads, using the dedicated PCA tools [52]. All the other graphs were generated using GraphPad Prism 7 (GraphPad Software, San Diego, California). Host pathway enrichment analysis and enrichment of transcription factor binding sites were performed using ShinyGO v0.60 (<http://bioinformatics.sdstate.edu/go/>) [53]. Due to poor annotation of *S. sonnei* Gene Ontology functions, we employed eggNOG-mapper v2 to annotate functions using orthologous assignments [54]. In total, 3918 *S. sonnei* protein sequences were retrieved from uniprot.org and scanned for orthologues. 2777 genes were assigned at least to one GO term. Out of the 1538 *S. sonnei* genes that were significantly differentially expressed, 860 were assigned to a least one GO term. Pathway enrichment analysis was performed for significantly differentially expressed genes in R, using the 'fgsea' Bioconductor package [55].

Statistical analysis and data processing

Except for graphs performed in R, all other graphs and statistical analyses were performed using GraphPad Prism 7. Statistical difference for survival curves were analysed using a Log-rank (Mantel-Cox) test. Differences in CFU recovery and gene expression levels were quantified on Log₁₀-transformed or Log₂-transformed data, respectively. To avoid Log(0), i.e., when no colonies were recovered, the CFU counts were assigned as 1. When only 2 groups were compared, significant differences were tested using an unpaired t-test at each timepoint. When more than 2 groups were compared, a one-way ANOVA with Sidak's correction was used. Unpaired t-test (comparison between 2 groups) or one-way ANOVA with Sidak's correction (comparison between more than 2 groups) was also applied to S3E Fig, Fig 5C and 5D, S5A and S5B Fig and Fig 6E and 6F but on non-transformed data, as in this case a

parametric distribution could be assumed. Statistics for categorical data were obtained by a two-sided *chi*-squared contingency test (S1D Fig, S6A Fig). For statistical quantification of immune cell numbers (non-parametric data), a two-tailed Mann-Whitney test (comparison between 2 groups) or a Kruskal-Wallis test with Dunn's correction (comparison between more than 2 groups) was used.

Supporting information

S1 Fig. (Related to Fig 1) S. sonnei is more virulent than S. flexneri in a zebrafish infection model. A,B. Dose response to S. sonnei infection. Survival curves (A) and Log₁₀-transformed CFU counts (B) of larvae injected in the HBV with increasing doses of *S. sonnei*. ~200 CFU range: 100–300 CFU (grey); ~600 CFU range: 400–700 CFU (blue); ~1500 CFU range: 1000–2000 CFU (green); ~5000 CFU: 4000–6000 CFU (red). Experiments are cumulative of 3 biological replicates. In B, full symbols represent live larvae and empty symbols represent larvae that at the plating timepoint had died within the last 16 hours. Statistics: Log-rank (Mantel-Cox) test (A); one-way ANOVA with Sidak's correction on Log₁₀-transformed data (B); ns, non-significant; ***p*<0.0021; *****p*<0.0001.

C-F. S. sonnei can disseminate from the injection site. Representative images of three larvae injected in the HBV with ~20000 CFU of GFP-labelled *S. flexneri* (C, compare to Fig 1E and 1F). The frequency of larvae with bacterial dissemination out of the HBV at 24 hpi is significantly higher for the *S. sonnei*-infected group when compared to the *S. flexneri* infected group (even when *S. flexneri* input is ~3-fold higher than *S. sonnei* input) (D). Survival curves (E) and Log₁₀-transformed CFU counts (F) of larvae injected in the HBV with ~7000 CFU *S. flexneri* (grey), ~20000 CFU of *S. flexneri* (blue) or ~7000 CFU *S. sonnei* (red). Experiments are cumulative of 3 biological replicates. In E, full symbols represent live larvae and empty symbols represent larvae that at the plating timepoint had died within the last 16 hours. Due to poor larval survival at 72 hpi, CFU data are available for < 3 larvae per biological replicate. Statistics: two-sided *chi*-squared contingency test (D); Log-rank (Mantel-Cox) test (E); one-way ANOVA with Sidak's correction on Log₁₀-transformed data (F); ns, non-significant; ***p*<0.0021; *****p*<0.0001. Scale bar = 1 mm.

G,H. S. sonnei is more virulent than S. flexneri in an intravenous infection model. Survival curves (G) and Log₁₀-transformed CFU counts (H) of larvae injected intravenously (IV, via the duct of Cuvier) with PBS (grey), *S. flexneri* (blue) or *S. sonnei* (red). Experiments are cumulative of 2 biological replicates. In H, full symbols represent live larvae and empty symbols represent larvae that at the plating timepoint had died within the last 16 hours. Statistics: Log-rank (Mantel-Cox) test (G); ns, non-significant; *****p*<0.0001.

I,J. A clinical isolate of S. sonnei is more virulent than a clinical isolate of S. flexneri. Survival curves (I) and Log₁₀-transformed CFU counts (J) of larvae injected in the HBV with *S. flexneri* isolate 2457T (blue) or *S. sonnei* isolate 381 (red). Experiments are cumulative of 3 biological replicates. In J, full symbols represent live larvae and empty symbols represent larvae that at the plating timepoint had died within the last 16 hours. Statistics: Log-rank (Mantel-Cox) test (I); unpaired t-test on Log₁₀-transformed data (J); ***p*<0.0021; *****p*<0.0001.

K-N. S. sonnei is more virulent than S. flexneri at 32.5°C and 37°C. Survival curves (K,M) and Log₁₀-transformed CFU counts (L,N) of larvae injected in the HBV with PBS (grey), *S. flexneri* (blue) or *S. sonnei* (red) at 32.5°C (K,L) or at 37°C (M,N). Experiments are cumulative of 2 biological replicates. In L,N, full symbols represent live larvae and empty symbols represent larvae that at the plating timepoint had died within the last 16 hours. Due to increased virulence of *S. sonnei* at 32.5°C (and poor survival of larvae at 24–72 hpi), CFU data are available for < 3 larvae per biological replicate for some experimental groups. ND: not determined.

Statistics: Log-rank (Mantel-Cox) test; **** $p < 0.0001$.
(PDF)

S2 Fig. (Related to Fig 2) Whole animal dual-RNAseq profiling of *S. sonnei* infected larvae.

A,B. Principal component analysis (PCA) of *S. sonnei* and zebrafish larvae transcriptomes. Analysis was performed on counts per million (CPM) reads values, using the dedicated PCA tools in R. Individual biological replicates (R1, R2, R3) for control (blue) and infected (red) conditions are reported. % in brackets indicate the variance of dimension explained by each principal component. Plot in A refers to *S. sonnei* genes and plot in B refers to zebrafish genes.

C,D. Boxplots representing the distribution of reads within the RNAseq libraries of each individual sample. Boxplots represent the sample median CPM reads with interquartile range, while whiskers indicate the 2.5–97.5 percentile range. Control samples are indicated in blue and infection samples are indicated in red. Biological replicates (R1, R2, R3) are also indicated. Plot in C refers to *S. sonnei* gene libraries and plot in D refers to zebrafish gene libraries.

E-H. Distribution histograms of significantly differentially expressed genes in *S. sonnei* and zebrafish larvae during infections. Each bar represents the number of significantly differentially expressed genes (repressed, blue (E,F); induced, red (G,H)) in each interval of $\text{Log}_2(\text{FC})$. Plots in E,G refer to *S. sonnei* genes, while plots in F,H refer to zebrafish genes.

I. Induction of well-established inflammatory markers in the RNAseq transcriptome. Bars indicate the average CPM reads for representative inflammatory marker. Compare to induction of same genes tested independently by qRT-PCR at the same timepoint in Fig 1D. Statistics: unpaired t-test on Log_2 -transformed data; ** $p < 0.0021$; *** $p < 0.0002$; **** $p < 0.0001$.

J. Pathway enrichment analysis of *S. sonnei* during infection *in vivo*. Pathway enrichment analysis was performed using eggNOG-mapper v2 to infer gene functions based on orthology. % are relative to all genes bioinformatically annotated to the pathway of interest. A variety of stress response processes are induced in *S. sonnei in vivo* in the zebrafish larvae, including amino acid and lipid metabolism, response to pH and ion homeostasis. Fractions flanking the histogram bars indicate the number of significantly affected genes in the pathway and the total number of genes annotated to the pathway in the library of reference.

K. Pathway enrichment analysis of *S. sonnei*-infected zebrafish larvae. Pathway enrichment analysis was performed using ShinyGO v0.60 (<http://bioinformatics.sdstate.edu/go/>). % are relative to all the genes bioinformatically annotated to the pathway of interest. A variety of immune-related processes are induced in zebrafish larvae in response to *S. sonnei* infection, including leukocyte (especially neutrophil) chemotaxis, response to cytokines and inflammation. Fractions flanking the histogram bars indicate the number of significantly affected genes in the pathway and the total number of genes annotated to the pathway in the library of reference.

(PDF)

S3 Fig. (Related to Fig 3) *S. sonnei* virulence depends on its O-antigen.

A,B. Schematic of *S. sonnei* and *S. flexneri*. Both *S. flexneri* and *S. sonnei* virulence plasmid encodes a type 3 secretion system (T3SS). However, differently than *S. flexneri*, *S. sonnei* virulence plasmid (pSS) encodes genes for the biosynthesis of a capsule and O-antigen (O-Ag) non-homologous to those of other *Escherichia* and *Shigella* species. *S. sonnei* additionally encodes a type 6 secretion system (T6SS) on the bacterial chromosome. The schematic in B also reports (in grey and between brackets) the name of the mutants used in the study.

C,D. Virulence of *S. sonnei* in zebrafish does not depend on the T6SS or capsule. Survival curves (C) and Log_{10} -transformed CFU counts (D) of larvae injected in the HBV with *S. sonnei* Δtssb (grey), Δg4c (blue), or WT (red) strains. Experiments are cumulative of 4 (C) or 3 (D) biological replicates. In D, full symbols represent live larvae and empty symbols represent

larvae that at the plating timepoint had died within the last 16 hours. Statistics: Log-rank (Mantel-Cox) test (C); one-way ANOVA with Sidak's correction on Log₁₀-transformed data (D); ns, non-significant.

E. *S. sonnei* virulence plasmid is maintained *in vivo* in zebrafish at 28.5°C. Larvae were injected with 1 nl (~7000 CFU) in the HBV with *S. flexneri* (blue) or *S. sonnei* (red) for 24 h at 28.5°C. Control bacteria (TSA plates) were spotted onto tryptic soy agar plates (10 µl of the bacterial inoculum/spot) and also grown for 24 h at 28.5°C. Bacteria were then harvested from larvae or plates and grown on Congo-Red plates at 37°C to quantify colonies that lost the virulence plasmid. Experiments are cumulative of 2 biological replicates. Statistics: one-way ANOVA with Sidak's correction; ns, non-significant; *p<0.0332; **p<0.0021.

F. Comparison of *S. sonnei* and *S. flexneri* O-antigen. *S. sonnei* 53G O-antigen has a unique sugar composition compared to the O-antigen of *S. flexneri* M90T. Figure legend abbreviations: AN: 2-Acetamido-2-deoxy-L-altruronic acid (L-AltNAc); FN: 2-Acetamido-4-amino-2,4-dideoxy-D-fucose (D-FucNAc); GN: 2-Acetamido-2-deoxy-D-glucose (D-GlcNAc); R: L-Rhamnose (L-Rha); G: D-Glucose (D-Glc); Ac: O-acetyl. Adapted from [56].

G. LPS blotting for *S. sonnei* strains used in this study. Crude LPS from WT, ΔO-Ag mutant, ΔO-Ag mutant complemented with plasmidic *S. sonnei* O-Ag (ΔO-Ag^{+pSSO-Ag}) and a strain cured from the pSS virulence plasmid (-pSS) were run on a 12% SDS-PAGE gel and blotted using an antibody specific to *S. sonnei* phase I O-Ag. Both the ΔO-Ag strain and the -pSS strain do not express the O-Ag, and plasmid reintroduction of the O-Ag synthesis genes partly restores O-Ag expression.

H-K. T3SS mutants and O-Ag mutants are attenuated *in vivo* at 32.5°C. Survival curves (H, J) and Log₁₀-transformed CFU counts (I,K) of larvae injected in the HBV with ΔO-Ag (grey), Δmxid (blue), or WT (red) *S. sonnei* at 32.5°C with either ~2000 (H,I) or ~6000 (J,K) CFU. Experiments are cumulative of 3 biological replicates. In I,K, full symbols represent live larvae and empty symbols represent larvae that at the plating timepoint had died within the last 16 hours. Due to increased virulence of *S. sonnei* at 32.5°C (and poor survival of larvae at 48–72 hpi) CFU data are available for < 3 larvae per biological replicate for some experimental groups. ND: not determined. Statistics: Log-rank (Mantel-Cox) test (H,J); unpaired t-test on Log₁₀-transformed data (I,K); ****p<0.0001.

L. Induction of the O-antigen chain length determinant protein *wzzB* *in vivo*. Dual-RNA-seq profiling shows that the *wzzB* is significantly upregulated in *S. sonnei* infected zebrafish. Bars indicate the average CPM reads. Statistics: unpaired t-test on Log₂-transformed data; ***p<0.0002.

M. Bacterial replication is necessary for death of zebrafish larvae. Survival curves of larvae injected in the HBV with heat killed ΔO-Ag (grey), heat killed WT (blue), live ΔO-Ag (green) or live WT (red) *S. sonnei*. Experiments are cumulative of 3 biological replicates. Bacterial input: ~6000 CFU. Statistics: Log-rank (Mantel-Cox) test; ns, non-significant; ****p<0.0001. (PDF)

S4 Fig. (related to Fig 4) *S. sonnei* O-antigen can counteract clearance by zebrafish neutrophils. A-C. Chemical ablation of macrophages. Representative images (A,B) and quantification (C) of macrophage ablation in *Tg(mpeg1:Gal4-FF)^{g125}/Tg(UAS-E1b:nfsB.mCherry)^{c264}* larvae which were treated with either Metronidazole (Mtz, macrophage ablated group, blue) or control DMSO vehicle (DMSO, red) prior to infection in the HBV with *S. sonnei*. Experiments are cumulative of 2 biological replicates. Statistics: two-tailed Mann-Whitney test; ****p<0.0001. Scale bars = 250 µm.

D,E. Macrophage ablation increases susceptibility to *S. flexneri*. Survival curves (D) and Log₁₀-transformed CFU counts (E) of *Tg(mpeg1:Gal4-FF)^{g125}/Tg(UAS-E1b:nfsB.mCherry)^{c264}*

larvae which were treated with either Metronidazole (Mtz, macrophage ablated group, blue) or control DMSO vehicle (DMSO, red) prior to infection in the HBV with *S. flexneri*. Experiments are cumulative of 3 biological replicates. In E, full symbols represent live larvae and empty symbols represent larvae that at the plating timepoint had died within the last 16 hours. Statistics: Log-rank (Mantel-Cox) test (D); unpaired t-test on Log₁₀-transformed data (E); ns, non-significant; *p<0.0332.

F-H. *pu.1* morpholino knockdown results in neutrophil depletion. Representative images (F,G) and quantification (H) of neutrophil depletion in *Tg(lyz:dsRed)^{nz50}* larvae injected with *pu.1* morpholino (blue) or control morpholino (red) at 1-cell stage. A significant ~3-fold decrease in neutrophil number can be observed at 3 dpf, prior to infection in the HBV with *S. sonnei*. Experiments are cumulative of 3 biological replicates. Statistics: two-tailed Mann-Whitney test; ****p<0.0001. Scale bars = 250 μm.

I,J. *pu.1* morpholino knockdown increases susceptibility to *S. sonnei* when infections are performed at 30 hpf. Survival curves (I) and Log₁₀-transformed CFU counts (J) of *pu.1* morphant (blue) or control (red) larvae infected in the HBV with WT *S. sonnei*. Experiments are cumulative of 3 biological replicates. In J, full symbols represent live larvae and empty symbols represent larvae that at the plating timepoint had died within the last 16 hours. To allow full ablation of immune cells by morpholino knockdown, infections are performed at 30 hpf. Statistics: Log-rank (Mantel-Cox) test; ****p<0.0001. (PDF)

S5 Fig. (related to Fig 5) *S. sonnei* can resist phagolysosome acidification and promote neutrophil cell death in an O-antigen-dependent manner. A,B. *S. sonnei* O-antigen contributes to acid tolerance *in vitro*. Growth curves of ΔO-Ag (blue) or WT (red) *S. sonnei*, cultured in tryptic soy broth adjusted to pH = 4 (A) or 6 (B). Statistics: unpaired t-test at the latest timepoint; ns, non-significant.

C. *S. sonnei* can replicate within phagosomes. Transmission electron micrograph of an infected phagocyte from zebrafish larvae at 3 hpi with WT *S. sonnei*, showing a dividing *S. sonnei* cell. Scale bar = 4 μm.

D. *S. sonnei* infection of zebrafish cell promotes morphological features of necrosis. Transmission electron micrograph of an infected neutrophil from a zebrafish larva at 3 hpi with WT *S. sonnei*, showing signs of necrotic cell death (arrowheads point at area of extranuclear chromatin degradation). Scale bar = 4 μm.

E. Pharmacological inhibition of necroptosis and/or apoptosis/pyroptosis does not protect zebrafish larvae. Survival curves of larvae which were treated with Necrostatin-1 (grey), Necrostatin-5 (blue), Q-VD-OPh (green), Necrostatin-1 + Q-VD-OPh (red) or control DMSO vehicle (black) upon infection in the HBV with *S. sonnei*. Experiments are cumulative of 3 biological replicates. Bacterial input: ~7000 CFU. Statistics: Log-rank (Mantel-Cox) test; ns, non-significant. (PDF)

S6 Fig. (related to Fig 7) Innate immunity can be trained to control *S. sonnei* *in vivo*. A,B. Response of 2dpf zebrafish embryos to sublethal dose (~80 CFU) of *S. sonnei*. Approximately 80% of WT GFP-*S. sonnei* injected embryos (and 100% of ΔO-Ag GFP-*S. sonnei* injected embryos) control infection (no detectable bacteria by fluorescence microscopy) by 48 hpi (A). Log₁₀-transformed CFU counts from controller larvae (no detectable bacteria by fluorescence microscopy) infected in the HBV with GFP-ΔO-Ag (blue) or WT (red) *S. sonnei*. Prior to receiving the secondary lethal dose (~8000 CFU) of mCherry-*S. sonnei*, ~80% of WT GFP-*S. sonnei* injected controllers (and 100% of ΔO-Ag GFP-*S. sonnei* injected controllers) cleared the primary infection (no CFU detectable from plating). Experiments are cumulative

of 4 (A) or 3 (B) biological replicates. Statistics: two-sided *chi*-square contingency test; **** $p < 0.0001$.

(PDF)

S1 Table. Differentially expressed *S. sonnei* genes and pathogen pathway enrichment analysis *in vivo*.

(XLSX)

S2 Table. Differentially expressed zebrafish genes and host pathway enrichment analysis in response to *S. sonnei* infection.

(XLSX)

S3 Table. Bacterial strains used in this study.

(PDF)

S4 Table. Primers and morpholinos used in this study.

(PDF)

Acknowledgments

We thank Margarida C. Gomes and Nagisa Yoshida for helpful discussion.

Author Contributions

Conceptualization: Vincenzo Torraca, Serge Mostowy.

Data curation: Myrsini Kaforou.

Formal analysis: Vincenzo Torraca, Myrsini Kaforou, Michael Hollinshead, Serge Mostowy.

Funding acquisition: Vincenzo Torraca, Serge Mostowy.

Investigation: Vincenzo Torraca, Gina M. Duggan, Hazel Guerrero-Gutierrez, Sina Krokowski, Michael Hollinshead.

Methodology: Myrsini Kaforou, Thomas B. Clarke, Rafal J. Mostowy, Gillian S. Tomlinson, Vanessa Sancho-Shimizu.

Resources: Jayne Watson, Vanessa Sancho-Shimizu, Abigail Clements.

Supervision: Myrsini Kaforou, Serge Mostowy.

Writing – original draft: Vincenzo Torraca, Serge Mostowy.

Writing – review & editing: Vincenzo Torraca, Serge Mostowy.

References

1. Khalil IA, Troeger C, Blacker BF, Rao PC, Brown A, Atherly DE, et al. Morbidity and mortality due to *Shigella* and enterotoxigenic *Escherichia coli* diarrhoea: the global burden of disease study 1990–2016. *Lancet Infect Dis*. 2018; 18: 1229–1240. [https://doi.org/10.1016/S1473-3099\(18\)30475-4](https://doi.org/10.1016/S1473-3099(18)30475-4) PMID: 30266330
2. Kotloff KL, Riddle MS, Platts-Mills JA, Pavlinac P, Zaidi AKM. Shigellosis. *Lancet*. 2018; 391: 801–812. [https://doi.org/10.1016/S0140-6736\(17\)33296-8](https://doi.org/10.1016/S0140-6736(17)33296-8) PMID: 29254859
3. Kotloff KL, Nataro JP, Blackwelder WC, Nasrin D, Farag TH, Panchalingam S, et al. Burden and aetiology of diarrhoeal disease in infants and young children in developing countries (the Global Enteric Multi-center Study, GEMS): A prospective, case-control study. *Lancet*. 2013; 382: 209–222. [https://doi.org/10.1016/S0140-6736\(13\)60844-2](https://doi.org/10.1016/S0140-6736(13)60844-2) PMID: 23680352
4. World Health Organization. Global priority list of antibiotic-resistant bacteria to guide research, discovery, and development of new antibiotics. WHO Press; 2017.

5. Baker KS, Dallman TJ, Field N, Childs T, Mitchell H, Day M, et al. Horizontal antimicrobial resistance transfer drives epidemics of multiple *Shigella* species. *Nat Commun*. 2018; 9: 1462. <https://doi.org/10.1038/s41467-018-03949-8> PMID: 29654279
6. Brinkmann V, Reichard U, Goosmann C, Fauler B, Uhlemann Y, Weiss DS, et al. Neutrophil extracellular traps kill bacteria. *Science*. 2004; 303: 1532–1435. <https://doi.org/10.1126/science.1092385> PMID: 15001782
7. Girardin SE, Boneca IG, Carneiro LAM, Antignac A, Jéhanno M, Viala J, et al. Nod1 detects a unique muropeptide from Gram-negative bacterial peptidoglycan. *Science*. 2003; 300: 1584–1587. <https://doi.org/10.1126/science.1084677> PMID: 12791997
8. Ogawa M, Yoshimori T, Suzuki T, Sagara H, Mizushima N, Sasakawa C. Escape of intracellular *Shigella* from autophagy. *Science*. 2005; 307: 727–731. <https://doi.org/10.1126/science.1106036> PMID: 15576571
9. Li P, Jiang W, Yu Q, Liu W, Zhou P, Li J, et al. Ubiquitination and degradation of GBPs by a *Shigella* effector to suppress host defence. *Nature*. 2017; 551: 378–383. <https://doi.org/10.1038/nature24467> PMID: 29144452
10. Wandel MP, Pathe C, Werner EI, Ellison CJ, Boyle KB, von der Malsburg A, et al. GBPs inhibit motility of *Shigella flexneri* but are targeted for degradation by the bacterial ubiquitin ligase IpaH9.8. *Cell Host Microbe*. 2017; 22: 507–518.e5. <https://doi.org/10.1016/j.chom.2017.09.007> PMID: 29024643
11. Krokowski S, Lobato-Márquez D, Chastanet A, Pereira PM, Angelis D, Galea D, et al. Septins recognize and entrap dividing bacterial cells for delivery to lysosomes. *Cell Host Microbe*. 2018; 24: 866–874.e4. <https://doi.org/10.1016/j.chom.2018.11.005> PMID: 30543779
12. Mostowy S, Bonazzi M, Hamon MA, Tham TN, Mallet A, Lelek M, et al. Entrapment of intracytosolic bacteria by septin cage-like structures. *Cell Host Microbe*. 2010; 8: 433–444. <https://doi.org/10.1016/j.chom.2010.10.009> PMID: 21075354
13. Pupo GM, Lan R, Reeves PR. Multiple independent origins of *Shigella* clones of *Escherichia coli* and convergent evolution of many of their characteristics. *Proc Natl Acad Sci*. 2000; 97: 10567–10572. <https://doi.org/10.1073/pnas.180094797> PMID: 10954745
14. Holt KE, Baker S, Weill F-X, Holmes EC, Kitchen A, Yu J, et al. *Shigella sonnei* genome sequencing and phylogenetic analysis indicate recent global dissemination from Europe. *Nat Genet*. 2012; 44: 1056–1059. <https://doi.org/10.1038/ng.2369> PMID: 22863732
15. Kotloff KL, Winickoff JP, Ivanoff B, Clemens JD, Swerdlow DL, Sansonetti PJ, et al. Global burden of *Shigella* infections: implications for vaccine development and implementation of control strategies. *Bull World Health Organ*. 1999; 77: 651–666. PMID: 10516787
16. Thompson CN, Duy PT, Baker S. The rising dominance of *Shigella sonnei*: an intercontinental shift in the etiology of bacillary dysentery. *PLoS Negl Trop Dis*. 2015; 9: e0003708. <https://doi.org/10.1371/journal.pntd.0003708> PMID: 26068698
17. Sack DA, Hoque AT, Huq A, Etheridge M. Is protection against shigellosis induced by natural infection with *Plesiomonas shigelloides*? *Lancet*. 1994; 343: 1413–1415. [https://doi.org/10.1016/s0140-6736\(94\)92531-3](https://doi.org/10.1016/s0140-6736(94)92531-3) PMID: 7910890
18. Anderson MC, Vonaesch P, Saffarian A, Marteyn BS, Sansonetti PJ. *Shigella sonnei* encodes a functional T6SS used for interbacterial competition and niche occupancy. *Cell Host Microbe*. 2017; 21: 769–776.e3. <https://doi.org/10.1016/j.chom.2017.05.004> PMID: 28618272
19. Torraca V, Mostowy S. Zebrafish infection: from pathogenesis to cell biology. *Trends Cell Biol*. 2018; 28: 143–156. <https://doi.org/10.1016/j.tcb.2017.10.002> PMID: 29173800
20. Gomes MC, Mostowy S. The case for modeling human infection in zebrafish. *Trends Microbiol*. 2019; <https://doi.org/10.1016/j.tim.2019.08.005> PMID: 31604611
21. Duggan GM, Mostowy S. Use of zebrafish to study *Shigella* infection. *Dis Model Mech*. 2018; 11: dmm032151. <https://doi.org/10.1242/dmm.032151> PMID: 29590642
22. Mostowy S, Boucontet L, Mazon Moya MJ, Sirianni A, Boudinot P, Hollinshead M, et al. The zebrafish as a new model for the *in vivo* study of *Shigella flexneri* interaction with phagocytes and bacterial autophagy. *PLoS Pathog*. 2013; 9: e1003588. <https://doi.org/10.1371/journal.ppat.1003588> PMID: 24039575
23. Willis AR, Moore C, Mazon-Moya M, Krokowski S, Lambert C, Till R, et al. Injections of predatory bacteria work alongside host immune cells to treat *Shigella* infection in zebrafish larvae. *Curr Biol*. 2016; 26: 3343–3351. <https://doi.org/10.1016/j.cub.2016.09.067> PMID: 27889262
24. Mazon-Moya MJ, Willis AR, Torraca V, Boucontet L, Shenoy AR, Colucci-Guyon E, et al. Septins restrict inflammation and protect zebrafish larvae from *Shigella* infection. *PLoS Pathog*. 2017; 13: e1006467. <https://doi.org/10.1371/journal.ppat.1006467> PMID: 28650995

25. Willis AR, Torraca V, Gomes MC, Shelley J, Mazon-Moya M, Filloux A, et al. *Shigella*-induced emergency granulopoiesis protects zebrafish larvae from secondary infection. *MBio*. 2018; 9. <https://doi.org/10.1128/mBio.00933-18> PMID: 29946048
26. Caboni M, Pédrón T, Rossi O, Goulding D, Pickard D, Citiulo F, et al. An O-antigen capsule modulates bacterial pathogenesis in *Shigella sonnei*. *PLoS Pathog*. 2015; 11: e1004749. <https://doi.org/10.1371/journal.ppat.1004749> PMID: 25794007
27. McVicker G, Tang CM. Deletion of toxin–antitoxin systems in the evolution of *Shigella sonnei* as a host-adapted pathogen. *Nat Microbiol*. 2017; 2: 16204. <https://doi.org/10.1038/nmicrobiol.2016.204> PMID: 27819667
28. Liu B, Knirel YA, Feng L, Perepelov A V., Senchenkova SN, Wang Q, et al. Structure and genetics of *Shigella* O-antigens. *FEMS Microbiol Rev*. 2008; 32: 627–653. <https://doi.org/10.1111/j.1574-6976.2008.00114.x> PMID: 18422615
29. François M, Le Cabec V, Dupont MA, Sansonetti PJ, Maridonneau-Parini I. Induction of necrosis in human neutrophils by *Shigella flexneri* requires type III secretion, IpaB and IpaC invasins, and actin polymerization. *Infect Immun*. 2000; 68: 1289–1296. <https://doi.org/10.1128/iai.68.3.1289-1296.2000> PMID: 10678940
30. Wang L, Wang Q, Reeves PR. The variation of O-antigens in Gram-negative bacteria. *Subcell Biochem*. 2010; 53: 123–152. https://doi.org/10.1007/978-90-481-9078-2_6 PMID: 20593265
31. Shepherd JG, Wang L, Reeves PR. Comparison of O-antigen gene clusters of *Escherichia coli* (*Shigella*) *sonnei* and *Plesiomonas shigelloides* O17: *sonnei* gained its current plasmid-borne O-antigen genes from *P. shigelloides* in a recent event. *Infect Immun*. 2000; 68: 6056–6061. <https://doi.org/10.1128/iai.68.10.6056-6061.2000> PMID: 10992522
32. Arts RJW, Moorlag SJCFM, Novakovic B, Li Y, Wang SY, Oosting M, et al. BCG vaccination protects against experimental viral infection in humans through the induction of cytokines associated with trained immunity. *Cell Host Microbe*. 2018; 23: 89–100.e5. <https://doi.org/10.1016/j.chom.2017.12.010> PMID: 29324233
33. Netea MG, Joosten LAB, Latz E, Mills KHG, Natoli G, Stunnenberg HG, et al. Trained immunity: a program of innate immune memory in health and disease. *Science*. 2016; 352: aaf1098–aaf1098. <https://doi.org/10.1126/science.aaf1098> PMID: 27102489
34. Ashkenazi S, May-Zahav M, Dinari G, Gabbay U, Zilberberg R, Samra Z. Recent trends in the epidemiology of *Shigella* species in Israel. *Clin Infect Dis*. 1993; 17: 897–899. <https://doi.org/10.1093/clinids/17.5.897> PMID: 8286636
35. Ashkenazi S. *Shigella* infections in children: New insights. *Semin Pediatr Infect Dis*. 2004; 15: 246–252. <https://doi.org/10.1053/j.spid.2004.07.005> PMID: 15494948
36. Ranjbar R, Soltan Dallal MM, Talebi M, Pourshafie MR. Increased isolation and characterization of *Shigella sonnei* obtained from hospitalized children in Tehran, Iran. *J Health Popul Nutr*. 2008; 26: 426–430. <https://doi.org/10.3329/jhpn.v26i4.1884> PMID: 19069621
37. Simon AK, Hollander GA, McMichael A. Evolution of the immune system in humans from infancy to old age. *Proc R Soc B Biol Sci*. 2015; 282: 20143085. <https://doi.org/10.1098/rspb.2014.3085> PMID: 26702035
38. Zhao L, Xiong Y, Meng D, Guo J, Li Y, Liang L, et al. An 11-year study of shigellosis and *Shigella* species in Taiyuan, China: active surveillance, epidemic characteristics, and molecular serotyping. *J Infect Public Health*. 2017; 10: 794–798. <https://doi.org/10.1016/j.jiph.2017.01.009> PMID: 28188118
39. Arts RJW, Joosten LAB, Netea MG. The potential role of trained immunity in autoimmune and autoinflammatory disorders. *Front Immunol*. 2018; 9: 298. <https://doi.org/10.3389/fimmu.2018.00298> PMID: 29515591
40. Butkeviciute E, Jones CE, Smith SG. Heterologous effects of infant BCG vaccination: potential mechanisms of immunity. *Future Microbiol*. 2018; 13: 1193–1208. <https://doi.org/10.2217/fmb-2018-0026> PMID: 30117744
41. Novakovic B, Messina NL, Curtis N. The heterologous effects of bacillus Calmette–Guérin (BCG) vaccine and trained innate immunity. *The Value of BCG and TNF in Autoimmunity*. 2018. pp. 71–90. <https://doi.org/10.1016/B978-0-12-814603-3.00006-9>
42. Datsenko KA, Wanner BL. One-step inactivation of chromosomal genes in *Escherichia coli* K-12 using PCR products. *Proc Natl Acad Sci*. 2000; 97: 6640–6645. <https://doi.org/10.1073/pnas.120163297> PMID: 10829079
43. Watson JL, Sanchez-Garrido J, Goddard PJ, Torraca V, Mostowy S, Shenoy AR, et al. *Shigella sonnei* O-antigen inhibits internalisation, vacuole escape and inflammasome activation. *bioRxiv*. 2019; 799379. <https://doi.org/10.1101/799379>

44. Standish AJ, Weiser JN. Human neutrophils kill *Streptococcus pneumoniae* via serine proteases. *J Immunol.* 2009; 183: 2602–2609. <https://doi.org/10.4049/jimmunol.0900688> PMID: 19620298
45. Tapper H, Sundler R. Bafilomycin A1 inhibits lysosomal, phagosomal, and plasma membrane H (+)-ATPase and induces lysosomal enzyme secretion in macrophages. *J Cell Physiol.* John Wiley & Sons, Ltd; 1995; 163: 137–144. <https://doi.org/10.1002/jcp.1041630116> PMID: 7896890
46. Prince LR, Bianchi SM, Vaughan KM, Bewley MA, Marriott HM, Walmsley SR, et al. Subversion of a lysosomal pathway regulating neutrophil apoptosis by a major bacterial toxin, pyocyanin. *J Immunol.* 2008; 180: 3502–11. <https://doi.org/10.4049/jimmunol.180.5.3502> PMID: 18292577
47. Curado S, Stainier DYR, Anderson RM. Nitroreductase-mediated cell/tissue ablation in zebrafish: a spatially and temporally controlled ablation method with applications in developmental and regeneration studies. *Nat Protoc.* 2008; 3: 948–954. <https://doi.org/10.1038/nprot.2008.58> PMID: 18536643
48. Roca FJ, Ramakrishnan L. TNF dually mediates resistance and susceptibility to mycobacteria via mitochondrial reactive oxygen species. *Cell.* 2013; 153: 521–534. <https://doi.org/10.1016/j.cell.2013.03.022> PMID: 23582643
49. Tyrkalska SD, Candel S, Angosto D, Gómez-Abellán V, Martín-Sánchez F, García-Moreno D, et al. Neutrophils mediate *Salmonella* Typhimurium clearance through the GBP4 inflammasome-dependent production of prostaglandins. *Nat Commun.* 2016; 7: 12077. <https://doi.org/10.1038/ncomms12077> PMID: 27363812
50. Levitte S, Adams KN, Berg RD, Cosma CL, Urdahl KB, Ramakrishnan L. Mycobacterial acid tolerance enables phagolysosomal survival and establishment of tuberculous infection *in vivo*. *Cell Host Microbe.* 2016; 20: 250–258. <https://doi.org/10.1016/j.chom.2016.07.007> PMID: 27512905
51. Love MI, Huber W, Anders S. Moderated estimation of fold change and dispersion for RNA-seq data with DESeq2. *Genome Biol.* 2014; 15: 550. <https://doi.org/10.1186/s13059-014-0550-8> PMID: 25516281
52. R Development Core Team. R: A language and environment for statistical computing. 2011.
53. Ge SX, Jung D. ShinyGO: a graphical enrichment tool for animals and plants. *bioRxiv.* 2018; 315150 <https://doi.org/10.1101/315150>
54. Huerta-Cepas J, Forslund K, Coelho LP, Szklarczyk D, Jensen LJ, Von Mering C, et al. Fast genome-wide functional annotation through orthology assignment by eggNOG-mapper. *Mol Biol Evol.* 2017; 34: 2115–2122. <https://doi.org/10.1093/molbev/msx148> PMID: 28460117
55. Sergushichev AA. An algorithm for fast preranked gene set enrichment analysis using cumulative statistic calculation. *bioRxiv.* 2016; 060012. <https://doi.org/10.1101/060012>
56. Anderson M, Sansonetti PJ, Marteyn BS. *Shigella* diversity and changing landscape: insights for the twenty-first century. *Front Cell Infect Microbiol.* 2016; 6: 45. <https://doi.org/10.3389/fcimb.2016.00045> PMID: 27148494